공학박사 학위논문

Autonomous Formation Flight of Multiple Unmanned Aerial Vehicles using Decentralized Communication

분산형 통신기법을 이용한 복수 무인기의 자동 편대비행

2016 년 2 월

서울대학교 대학원

기계항공공학부

박 철 우

Abstract

To perform surveillance or reconnaissance of large areas effectively and efficiently, the use of multiple unmanned aerial vehicles (UAVs) flying in formation is recommended. For formation flight, a guidance and control algorithm is required. Recently, many studies have been conducted to develop algorithms for formation flight, but no centralized communication structure that is suitable for multiple UAV formation flight has become widely used. Additionally, the performance of the developed algorithms has mainly been demonstrated using numerical simulations or ground robots, which do not reflect the dynamic characteristics of UAVs. In this dissertation, a formation flight algorithm based on decentralized communication is proposed, and the performance of the proposed algorithm is verified by numerical simulations and a flight test experiment.

In this study, a multiple UAV system is constructed, and a formation guidance algorithm is proposed, and its use is demonstrated in an autonomous formation flight. To develop the multiple UAV platform, a UAV hardware system, including the airframe and avionics, is constructed. An on-board decentralized information sharing method is proposed, and the effect of the communication delay is analyzed. Based on sensor information sharing, a law for guiding multiple UAVs as they perform circular and close formations is designed. Numerical simulations are performed to demonstrate the performance of the formation flight guidance and control algorithm for multiple UAVs. Finally, a flight test is performed to verify the proposed algorithm for guiding the formation flight of a multiple-UAV system.

Keywords: Multiple UAVs, Formation flight, Decentralized communication, Close formation flight, Triangular formation.

Student number: 2009-20683

Table of Contents

ABSTRACT ..... **I**

TABLE OF CONTENTS ..... **III**

LIST OF TABLES ..... **V**

LIST OF FIGURES ..... **VII**

1. INTRODUCTION **1**

1.1 BACKGROUND AND OBJECTIVE 1

1.2 APPROACH AND CHALLENGES 3

1.3 CONTRIBUTIONS 8

1.4 DISSERTATION OUTLINE 9

2. MULTIPLE UAV SYSTEM **11**

2.1 AIRFRAME DEVELOPMENT 11

2.2 AVIONICS 14

2.3 ONBOARD DECENTRALIZED COMMUNICATION 19

2.4 UAV MODELING AND SIMULATION SETUP 27

3. FORMATION FLIGHT GUIDANCE **33**

3.1 CIRCULAR FORMATION FLIGHT GUIDANCE 33

3.2 CLOSE FORMATION FLIGHT GUIDANCE 41

3.2.1 Behavioral Approach based Formation Flight Guidance 41

3.2.2 Leader-Follower Approach based Formation Flight Guidance 55

4. INTEGRATED FORMATION FLIGHT SIMULATION **75**

4.1 PROCEDURE FOR AUTONOMOUS FORMATION FLIGHT 75

4.1.1 Circular Formation Flight with Separated Altitude 78

4.1.2 Circular Formation Flight at the Same Altitude 78

4.1.3 Separation and Reconfiguration Formation Flight 78

4.1.4 Close Circular Formation Flight 79
4.1.5 Close Triangular Formation Flight 79
4.2 SIMULATION RESULTS 80

5. EXPERIMENTAL RESULT 85

6. CONCLUSION 95

6.1 CONCLUDING REMARKS 95
6.2 FUTURE RESEARCH DIRECTIONS 96

BIBLIOGRAPHY 97

List of Tables

Table 2.1: Specifications of the developed UAV 12
Table 2.2: Specifications of the developed embedded FCC 15
Table 2.3. Specifications of the avionics 17
Table 2.4: Comparison of the wireless technology standards 20
Table 2.5: Communication packets of the multiple UAVs 21
Table 3.1: Initial simulation parameters of the circular formation guidance.. 39
Table 3.2: Initial simulation parameters (the suggested FGC method @ t_{com} = 0.02 s) 47
Table 3.3: Initial simulation parameters (the suggested FGC method @ t_{com} = 1.00 s) 51
Table 3.4: Initial simulation parameters (the suggested Leader- follower method @ t_{com} = 0.02 s) 59
Table 3.5: Initial simulation parameters (the suggested Leader- follower @ t_{com} = 1.00 s) 64
Table 3.6: Initial simulation parameters (the suggested Leader- follower method @ t_{com} = 1.00 s with position estimation of UAV1) 69
Table 4.1: The integrated formation flight scenarios 76
Table 4.2: Initial parameters of the integrated formation flight simulation 80

List of Figures

Figure 1.1: (a) Circular formation flight (b) Close formation flight 2
Figure 1.2: High-bandwidth centralized control 4
Figure 1.3: Low-bandwidth decentralized control 4
Figure 1.4: The virtual structure approach 5
Figure 1.5: The behavioral approach (using the formation geometry center method)) 5
Figure 1.6: The leader-follower approach 5
Figure 1.7: A triangular formation flight during the integrated formation flight 9
Figure 2.1: The Selected off-the-shelf airframe (a) storage (b) deployment .. 12
Figure 2.2: (a) NextEngine 3D scanner (b) CubeX Duo 3D printer 13
Figure 2.3: (a) 3D scanning of original airframe canopy (b) 3D canopy reconstruction (c) redesigned canopy including AOA, AOS, and pitot-static tube mount (d) 3D printing result..... 14
Figure 2.4: The developed embedded FCC..... 15
Figure 2.5. Avionics setup 16
Figure 2.6: Avionics connection diagram..... 17
Figure 2.7: Avionics installations of the UAV..... 18
Figure 2.8: Developed three identical UAVs..... 18
Figure 2.9: Communication failure because of simultaneous transmission ... 20
Figure 2.10. Description of the sequential cyclic communication 22
Figure 2.11. Communication flow of the two UAVs..... 22
Figure 2.12: Communication delay of ZigBee between UAV1 and UAV2.... 24
Figure 2.13: Test setup of the sequential cyclic communication..... 25
Figure 2.14: A sequential communication structure..... 26
Figure 2.15: Test result of sequential cyclic communication 27
Figure 2.16: Sequence of lateral system identification flight..... 28
Figure 2.17: Result of the lateral system model estimation 30

Figure 2.18: Result of the longitudinal system model estimation 31
Figure 2.19: Simulation configuration of MATLAB/Simulink 32
Figure 3.1: The nonlinear path-following guidance algorithm 34
Figure 3.2: Lateral acceleration relationship 35
Figure 3.3: Phase angles on the circular path 35
Figure 3.4: Description of lateral controller 38
Figure 3.5: Description of longitudinal controller 38
Figure 3.6: Simulation results of the circular formation guidance 40
Figure 3.7: Suggested FGC guidance: formation keeping 42
Figure 3.8: Formation geometry of the suggested FGC formation 43
Figure 3.9: Suggested FGC guidance: formation path following 44
Figure 3.10: Formation keeping and path following of the suggested FGC guidance 44
Figure 3.11: Description of the combined path of *i*-th UAV 45
Figure 3.12: Simulation results of the suggested FGC formation algorithm (trajectories of UAVs @ t_{com} = 0.02 s) 48
Figure 3.13: Simulation results of the suggested FGC formation algorithm (formation positions @ t_{com} = 0.02 s) 49
Figure 3.14 Simulation results of the suggested FGC formation algorithm (formation position errors @ t_{com} =0.02 s) 50
Figure 3.15: Simulation results of the suggested FGC formation algorithm (trajectories of UAVs @ t_{com} = 1.00 s) 52
Figure 3.16: Simulation results of the suggested FGC formation algorithm (formation positions @ t_{com} = 1.00 s) 53
Figure 3.17: Simulation results of the suggested FGC formation algorithm (formation position errors @ t_{com} = 1.00 s) 54

Figure 3.18. Suggested formation path generation algorithm of the follower UAV 55
Figure 3.19: Formation geometry of the leader-follower formation 59
Figure 3.20: Simulation results of the suggested leader-follower formation algorithm (trajectories of UAVs @ t_{com} = 0.02 s) 60
Figure 3.21: Simulation results of the suggested leader-follower formation algorithm (formations positions @ t_{com} = 0.02 s) 61
Figure 3.22: Simulation results of the suggested leader-follower formation algorithm (formation position errors @ t_{com} = 0.02 s) 62
Figure 3.23: Standard deviation of position error depending on longitudinal formation distance @ $y_{body} = 15m$ 63
Figure 3.24: Standard deviation of position error depending on lateral formation distance @ $x_{body} = 15m$ 63
Figure 3.25: Simulation results of the suggested leader-follower formation algorithm (trajectories of UAVs @ t_{com} = 1.00 s) 65
Figure 3.26: Simulation results of the suggested leader-follower formation algorithm (formation positions @ t_{com} = 1.00 s) 66
Figure 3.27: Simulation results of the suggested leader-follower formation algorithm (formation position errors @ t_{com} = 1.00 s) 67
Figure 3.28: Formation position errors depending on t_{com} 68
Figure 3.29: Communication delay compensation 68
Figure 3.30: Simulation results of the suggested leader-follower formation algorithm (trajectories of UAVs @ t_{com} = 1.00 s with position estimation of UAV1) 70

Figure 3.31: Simulation results of the suggested leader-follower formation algorithm (formation positions @ t_{com} = 1.00 s with position estimation of UAV1) 71
Figure 3.32: Simulation results of the suggested leader-follower formation algorithm (formation position errors @ t_{com} = 1.00 s with position estimation of UAV1) 72
Figure 3.33: Formation position errors depending on communication period with position estimation of the leader UAV 73
Figure 4.1: A flight path description of the integrated formation flight scenarios 77
Figure 4.2: 2D and 3D simulation results of the integrated formation flight . 81
Figure 4.3: Simulation results of the circular formation flight..... 82
Figure 4.4: Simulation results of the close triangular formation flight 83
Figure 5.1: 2D and 3D results of the integrated formation flight test (a) Sequential takeoff, (b) Circular formation with separate altitude, (c) Circular formation with same altitude..... 87
Figure 5.2: 2D and 3D results of the integrated formation flight test (a) Separation and reconfiguration of circular formation, (b) Reconfiguration of circular formation, (c) close circular formation 88
Figure 5.3: 2D and 3D results of the integrated formation flight test (a) Transition to close formation, (b) Close triangular formation, (c) Sequential landing..... 89
Figure 5.4: Detail results of the close triangular formation flight..... 91
Figure 5.5: Position histories of the integrated formation flight 92
Figure 5.6: Command histories of the integrated formation flight..... 93
Figure 5.7: Flight experiment setup 94
Figure 5.8: Multiple UAVs in close triangular formation 94

1. Introduction

1.1 Background and Objective

Recently, many studies of multiple UAVs undertaking various missions have been conducted to address the increasing demand for applications of unmanned aerial vehicles (UAVs) [1-10]. The merits of using multiple UAVs are that they can monitor multiple targets simultaneously and that multiple agents can complement each other in response to failures. To operate multiple UAVs, a formation flight guidance law should be implemented. A formation flight guidance law enables each UAV to maintain its relative position in the formation, which allows the UAVs to be efficiently and safely controlled while they perform their mission satisfactorily.

Depending on its geometry, a formation flight can be classified as a circular formation flight or a close formation flight. In this study, formations such as swarms are not considered because they does not have definite formation geometries. A group of UAVs typically performs a circular formation flight around an area in a large-area monitoring mission, as shown in Fig. 1.1(a). In a circular formation, multiple UAVs control the phase angles between the UAVs to make the surveillance more efficient. However, when the UAVs move to the next mission area, they should gather and perform a close formation flight to reduce the total aerodynamic drag and increase their survivability, as shown in Fig. 1.1(b). Therefore, both formations are required in various multiple UAV missions. Each formation guidance law has been widely studied and verified by numerical simulations or flight tests. Formation flight guidance algorithms, including the standoff tracking [11], coordinated formation [12], and formation reconfiguration [13] algorithms, have been introduced and verified using numerical simulations. Formation flight tests have been conducted using two fixed-wing UAVs [14], three fixed-wing UAVs [15], and three rotary-wing UAVs [16].

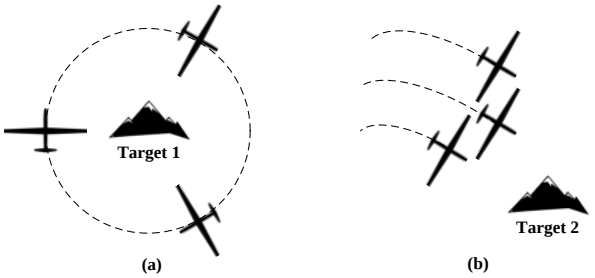

Figure 1.1: (a) Circular formation flight (b) Close formation flight

Usually, formation flight algorithms are developed under the assumption that each UAV is a 3 degree-of-freedom (DOF) point mass. In this case, the performance of the proposed guidance logic may be degraded when it is applied to a fixed-wing UAV because the real flight dynamics are not considered. In contrast, the results of the simulation may differ from the actual formation flight because perfect information sharing between multiple UAVs is assumed. When they perform a formation flight, in contrast to the simulation environment, the multiple UAVs should share information via a wireless communication device that has a communication delay. Especially during a close formation flight, a communication delay could cause the formation to fail, and therefore, the delay should be analyzed in detail. In summary, a formation flight guidance law that considers UAV dynamics and communication delays should be developed. In addition, the developed algorithm should be tested in a simulation environment that considers the communication limits.

In flight test experiments, if a ground control station (GCS) is mainly used to relay information between UAVs, then, it could be the single point at which the formation fails. Moreover, information on all the UAVs is collected by the GCS and retransmitted to the UAVs; therefore, there is a large communication load and an additional communication delay, which makes precise formation flight more difficult. In addition, the range of the mission is limited to the communication boundary around the GCS. To avoid using a centralized GCS, the UAVs should be directly interconnected using a multipoint-to-multipoint

topology for exchanging information. A multipoint-to-multipoint topology requires decentralized connections between the UAVs. However, a communications system supporting this topology requires an expensive and complex radio frequency (RF) system. The system also consumes a large amount of power, which is usually not suitable for small-scale UAV applications. Therefore, to perform a formation flight using a small UAV system, the communications system should be carefully designed by considering a multipoint communication topology and reducing its weight, power, and latency.

Motivated by these issues, a decentralized multiple UAV communications system for formation flight is developed, and formation flight guidance algorithms are proposed. To resolve the above issues, from the early stages of this study, the development of the multiple UAV system and the design of the algorithms are conducted simultaneously while the characteristics of fixed-wing UAVs and the limits on communication during formation flight are considered. To validate the formation flight guidance algorithms, an integrated formation flight consisting of various formation flight scenarios is conducted.

The objective of this study is to propose formation flight algorithms and to validate their performance using an integrated formation flight test involving three small fixed-wing UAVs.

1.2 Approach and Challenges

Formation control is directly related to communication structures, which are important in formation flight. Usually, a formation can be controlled using a centralized or decentralized control scheme. In a centralized control scheme, all information is concentrated at a central GCS or the central leader, as shown in Fig. 1.2, and a single agent controls the entire formation. Theoretically, centralized control schemes perform best and easily control each UAV. However, centralized control requires a high-bandwidth communication link

and has a high computational cost at the central point. In addition, failure of the central point may cause the entire formation to fail. Furthermore, if a GCS is the central point, the mission range is limited to the communication range between the GCS and the formation.

In contrast, in a decentralized control scheme, each UAV is able to make decisions about the formation, and there is no central control point, as shown in Fig. 1.3. The formation survive a partial UAV loss, which frequently occurs in small UAV operations, and the remaining UAVs can complete the mission. Because there is no centralized communication point, decentralized control requires a lower bandwidth communication link than centralized control does. Because the communication bandwidth depends on the performance of the wireless device, a low-bandwidth communication link can be created using a relatively small device. Because of these advantages, decentralized control is suitable for the formation flight of small UAVs.

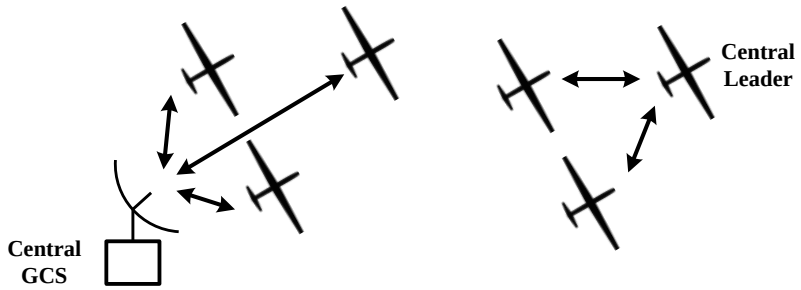

Figure 1.2: High-bandwidth centralized control

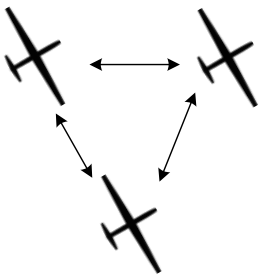

Figure 1.3: Low-bandwidth decentralized control

In contrast, formation flight guidance algorithms are divided into three categories: virtual structure formation guidance, behavioral formation guidance, and leader-follower formation guidance. The main differences between these approaches are in what they use as a reference formation, as shown in Figs. 1.4-1.6.

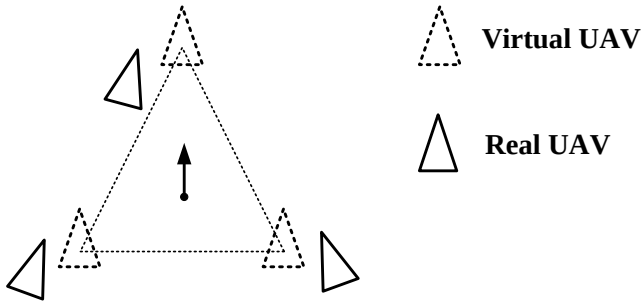

Figure 1.4: The virtual structure approach

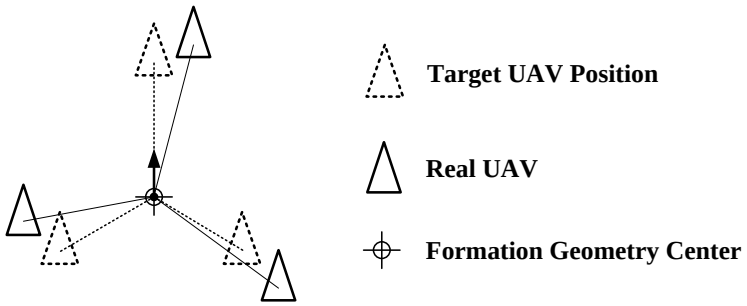

Figure 1.5: The behavioral approach (using the formation geometry center method))

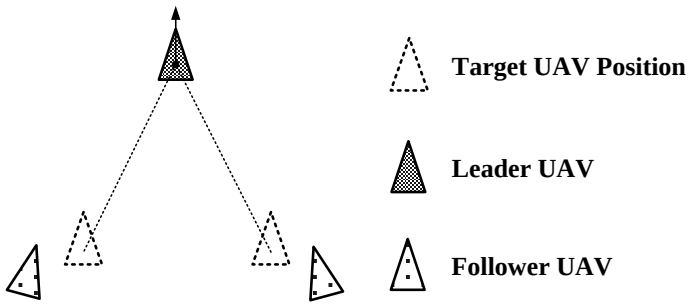

Figure 1.6: The leader-follower approach

In the virtual structure approach, the formation is considered a single rigid structure, as shown in Fig. 1.4. Because there is no physical reference formation, the formation is maintained regardless of the loss of individual UAVs. The generation of guidance commands is fairly simple, and therefore, it is suitable for large formations. Additionally, the behavior of the formation can be easily described mathematically. However, the virtual structure approach does not have formation feedback, and the formation may fail when a UAV cannot follow the virtual UAV because the selected virtual point is too far away or there is a strong headwind in the mission area. Moreover, all the UAVs in the formation should follow the same virtual structure, which means the virtual structure should be controlled at a central point. Therefore, a centralized control scheme is unavoidable in this approach.

In the behavioral approach, for a given formation pattern, a guidance command is generated from the weighted sum of each UAV's behavior. Figure 1.5 shows the formation geometry center (FGC) method, which is a typical realization of the behavioral approach. The FGC point is determined from the positions of all the UAVs, and each UAV is required to maintain a specific position relative to FGC. Inherently, this approach has formation feedback ability and uses a decentralized control scheme. However, the behavioral approach requires all the UAVs to compute the FGC point from synchronized positions, and therefore, the FGC can oscillate if there are communication delays. This may cause the entire formation to oscillate, which can cause collisions between UAVs in close formation flights.

In the leader-follower approach, the lead UAV follows the target trajectory, and the other UAVs follow the leader while maintaining their relative distances, as shown in Fig. 1.6. This approach has the advantage of simple decision making because each follower's position is determined simply by considering the leader's state. The leader-follower approach has also several disadvantages, such as being a centralized control approach. However, by implementing decentralized communication logic, decentralized control-based leader-

follower formation flight can be achieved. The leader and the UAVs that follow it can communicate in both directions, not only one. This feature enables formation feedback, including collision avoidance, between the UAVs. In addition, because the lead UAV is monitored, its failure can be detected. Note that the formation geometry is only determined by the leader's position, and therefore, a communication delay can be easily compensated for using correct estimates of the leader's position. For these reasons, in this study, the leader-follower approach is selected as the main method behind the close formation algorithm, and the developed algorithm is verified by numerical simulations and a flight test.

In contrast, circular formation flight can be performed by controlling the phase angles of the UAVs on the circular path [17]. The target phase angles are determined by the number of UAVs in the circular path. During circular formation flight, decentralized control is also useful for calculating the phase angles and reshaping the formation. In this study, close and circular formation flight algorithms are developed separately, and they are verified by an integrated formation flight.

The technical challenges of the close formation flight algorithm are as follows:

- Generating guidance commands to maintain the formation geometry and to follow the formation path simultaneously.
- Compensating for the communication delay when information is shared.

The technical challenges of flight demonstration are as follows:

- Implementing a bidirectional and multipoint-to-multipoint communication topology.
- Designing an integrated formation flight that includes multiple formations.

1.3 Contributions

This study's contributions to autonomous formation flight are summarized as follows:

- For close formation flight, a leader-follower-based formation guidance algorithm is proposed. This dissertation describes the path-following guidance laws of the behavioral approach and the leader-follower approach. The performance is analyzed with the assumption that there is a limit on communication.

- A bidirectional, multipoint-to-multipoint communication structure is developed and implemented for a small multiple UAV system. The communication delay between the UAVs is analyzed, and the information shared between the four UAVs is updated at 10 Hz in the avionics system developed.

- An integrated formation flight is successfully performed. Circular and close formation flights are performed sequentially. In the integrated formation flight, formation separation and reconfiguration are also performed. Therefore, the developed algorithms are applicable to various formation flight missions. Additionally, a triangular close formation flight of three UAVs is performed as shown in Fig. 1.7.

Figure 1.7: A triangular formation flight during the integrated formation flight

1.4 Dissertation Outline

This dissertation is organized as follows:

Chapter 2 describes the experimental multiple UAV system. Three UAVs and a ground monitoring system are developed, and a decentralized communication structure is realized. The effect of the time delay in the communications system is analyzed. System identification of the UAVs is performed, and a simulated multiple UAV environment is introduced.

Chapter 3 discusses the formation flight guidance logic. Nonlinear path-following guidance is used to ensure that the UAVs maintain the formation geometry during flight and that they follow a mission trajectory. The effect of the communication delay are simulated for various approaches to formation guidance. Circular formation guidance is also introduced.

Chapter 4 describes integrated formation flight. To enable the UAVs to perform an autonomous formation flight and to handle various formation missions, the concept of integrated formation flight is introduced. An integrated formation flight comprises five modes of formation during a mission, including

formation separation, formation reconfiguration and close formation. Each mode is automatically changed by a consensus of the UAVs. The concept of integrated formation flight is verified by simulation.

Chapter 5 describes the results of the formation flight test. Circular formation flight and close formation flight are performed during an integrated formation flight.

Chapter 6 summarizes the conclusion and directions for future research.

2. Multiple UAV System

This chapter describes the development of experimental multiple UAV system, which includes airframe selection, avionics, communication system, and modeling of UAV [18]. The performance of formation flight is closely related with an UAV hardware as well as a formation guidance logic. The main development issue is to construct identical multiple UAVs with intercommunicating between UAVs. Without considering an identical multiple UAVs development, separately developed UAVs have a different flight characteristics, and therefore the performance of formation flight can be degraded.

Decentralized control structure requires information of other UAV, and therefore multiple UAVs should be able to communicate with other UAVs. A simulation environment of multiple UAVs is also required using the mathematical models of target UAV for verifying a developed algorithm.

In this chapter, the development of multiple UAV system is explained. First, the target airframe is selected with consideration of multiple UAV operation, and avionic system is mounted on airframe using 3D printed canopy. Onboard information sharing scheme is implemented and analyzed for decentralized communication between UAVs. A system identification is also performed to determine lateral and longitudinal system models of UAV. Finally, multiple UAV simulation environment is described.

2.1 Airframe Development

In selection of the UAV airframe, robustness and portability are mainly considered due to frequent take-off and landing of more than three UAVs. A wooden airframe is not suitable in this situation. Instead, an EPO (Expanded Ploy Ethylene)/ EPP (Expanded Poly Propylene) airframe is proper because of its durable and detachable characteristics. Pusher-type airplane is preferred for

AOA (Angle of Attack), AOS (Angle of Sideslip), and pitot-static airspeed sensor configuration. A glider-type aircraft is also preferred rather than an acrobatic-type aircraft, because formation flight requires long flight time. For these reasons, an off-the-shelf RC airplane (Hitec Skyscout) shown in Fig. 2.1 has been selected in this study, which is made up of durable EPO material and has a pusher-type configuration with folding prop, to ensure uniform and reliable flight characteristics of the UAVs [19]. It also has detachable main wing and tail wing for compact storage and easy transportation. Detail specification of the selected UAV is summarized in Table 2.1.

Table 2.1: Specifications of the developed UAV

Characteristics	Range	Performance	Range
Length	980 mm	Endurance	25 min
Wingspan	1384 mm	Cruise speed	11 m/s
Dry weight	694 g	Maximum Thrust	2.5 N
Gross weight	810 g	Mission altitude	60 m
Battery capacity	11.1V, 2200mAh	Operation range	1 km

(a) **(b)**

Figure 2.1: The Selected off-the-shelf airframe (a) storage (b) deployment

The selected airframe has a detachable canopy in front of fuselage, and therefore it is suitable for avionic system mounting. However, the canopy has an arbitrary shape, and mounting the avionics is neither easy nor reproducible. Typically, off-the-shelf airframes have avionics mounting problem. To solve this problem, 3D scanner and 3D printer in Fig. 2.2 are used to design a canopy containing avionic system in it. Development steps of redesigning canopy are described in Fig. 2.3. The 3D scanner captures still images of an original canopy as shown in Fig. 2.3(a), and processing software generates a 3D canopy model as shown in Fig. 2.3(b). Based on the acquired 3D canopy model, the canopy is redesigned for correct mounting of FCC (Flight Control Computer), AOA, AOS, and pitot-static airspeed sensors as shown in Fig. 2.3(c). Finally, the redesigned canopy is printed out using the 3D printer as shown in Fig. 2.3(d). This procedure makes every multiple UAV have an identical avionics mounting geometry. By this procedure, AOA, AOS, and pitot-static airspeed sensors could be correctly installed.

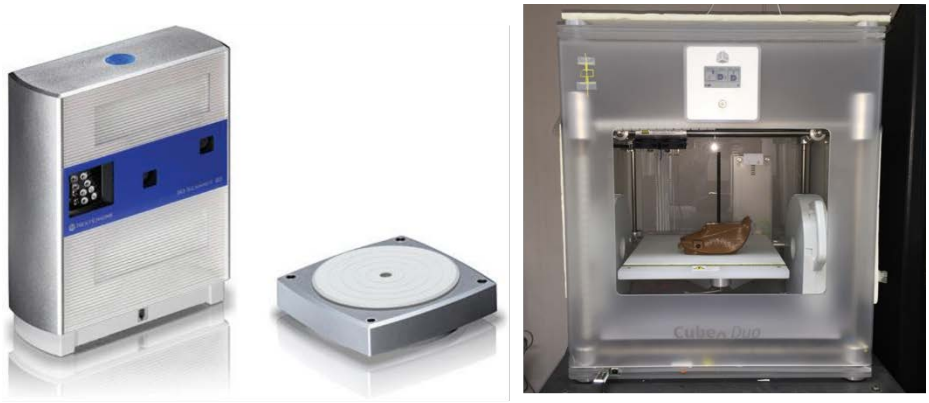

(a) **(b)**

Figure 2.2: (a) NextEngine 3D scanner (b) CubeX Duo 3D printer

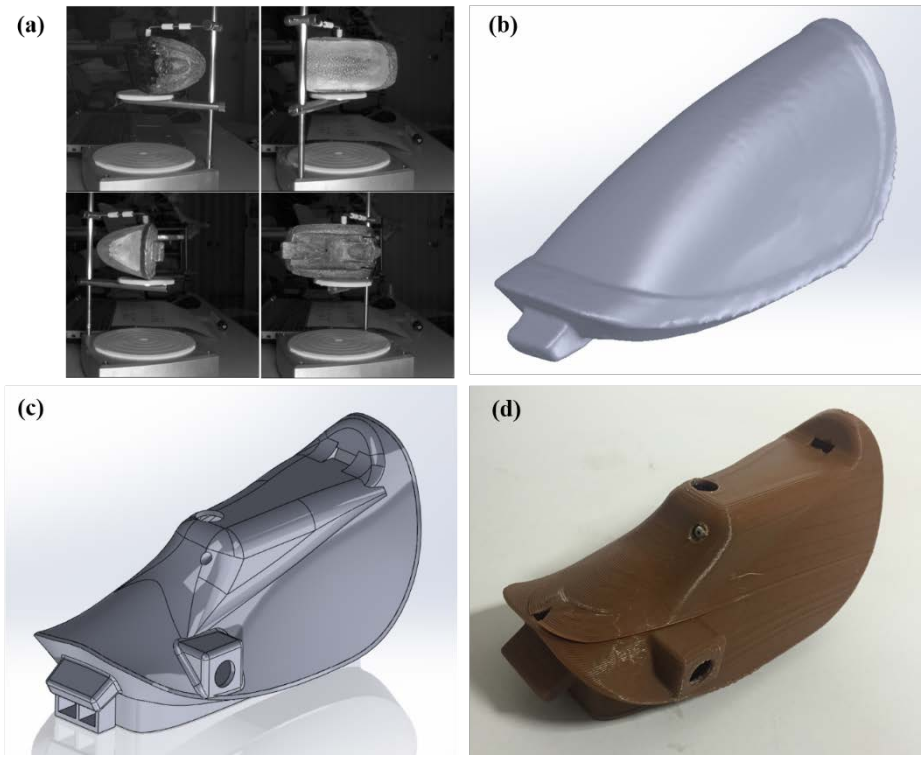

Figure 2.3: (a) 3D scanning of original airframe canopy (b) 3D canopy reconstruction (c) redesigned canopy including AOA, AOS, and pitot-static tube mount (d) 3D printing result

2.2 Avionics

The avionics, the electronic systems for the aircraft, enables an airframe to perform autonomous flight. In the avionics system, a flight control computer is a core part, because FCC calculates a guidance algorithm and controls an entire UAV system including sensors, actuator, and telemetry. There are numerous off-the-shelf FCCs in commercial market, but there are limitations when FCC is applied to the development of the multiple UAV system. A small-size FCC having multiple communication ability is required for the formation flight, but most commercial FCCs only support a point to point communication. In case of the multiple communication, large installation space or additional central

router is required. For these reason, the embedded FCC as shown in Fig. 2.4 has been developed to realize the multiple communication topology. The developed ARM Cortex-M3-based embedded FCC controls the control surfaces of the UAV, and especially an onboard ZigBee modem communicates with the other UAVs. The specification of FCC is summarized in Table 2.2. Based on the embedded FCC, the developed UAV is equipped with multiple sensors to achieve precise flight control.

Figure 2.4: The developed embedded FCC

Table 2.2: Specifications of the developed embedded FCC

Characteristic	Value
Dimension	71 x 31 x 17 mm
Weight	24 g
Processor	2 x STM32F103 @ 72 MHz
Telemetry	XBP09-DMUIT-156
Interface	1 x I2C, 1 x UART, 3 x ADC
Operating voltage	6 V ~ 18 V
Power consumption	1.4W @ 200 mA
Description	Dual processor configuration 6 channel PWM in & out Differential pressure sensor Barometric pressure sensor 3 channel 12 bit ADC Expansion I2C port

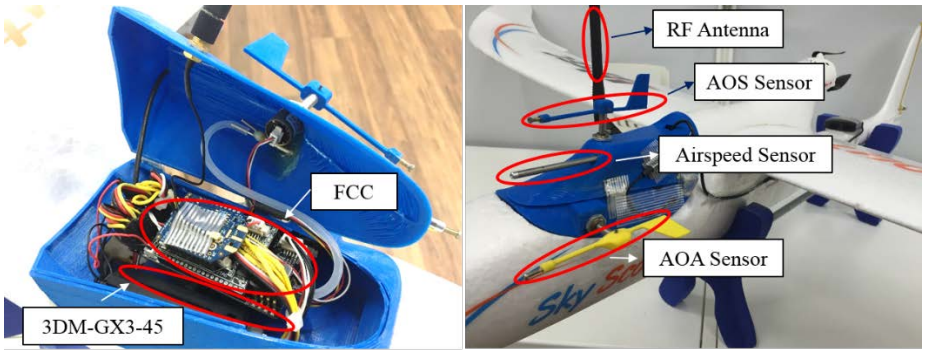

Figure 2.5. Avionics setup

Figure 2.5 shows the avionics setup in the UAV using the redesigned canopy. A microstrain 3DM-GX3-45 inertial navigation sensor is used as an inertial navigation system (INS) to measure the vehicle attitude, position, and velocity. The external high-gain GPS antenna of the 3DM-GX3-45 is located at the tail of the UAV. A US Digital MA3 miniature absolute magnetic encoder is used to measure the angle of attack (AOA) and angle of sideslip (AOS), which are relative to the direction of the wind. This miniature encoder sensor provides an absolute rotation angle based on a non-contact method with low friction; therefore, it is appropriate for measuring wind direction in a small-scale low airspeed UAV. Offset errors of AOA, AOS sensor are calibrated after installation. A pitot-static tube is connected to a MPX7002 differential pressure sensor to measure the relative wind speed. The measured dynamic pressure is converted to air speed. A XBP09-DMUIT-156 Zigbee modem is selected as a communication device because it supports multipoint-to-multipoint communication. The avionics specifications are summarized in Table 2.3.

All of the avionics components are connected to the developed embedded FCC. Figure 2.6 shows the connection diagrams of avionics. All sensors are mounted at detachable canopy, and therefore the avionics can be easily replaced with spare canopy in case of avionics failure. Figure 2.7 shows the installed avionics in the developed UAV.

Table 2.3. Specifications of the avionics

Component	Model name	Data rate	Specification
FCC	ARM FCC-M3	400 Hz	ARM Cortex-M3, 72 MHz Clock, 6 Ch PWM In & Out
Inertial navigation sensor	3DM-GX3-45	50 Hz	Typ. Attitude accuracy ± 0.35 deg Typ. Velocity accuracy ± 0.1 m/s Typ. Position accuracy ± 2.5 m RMS
AOA, AOS sensor	3MA-A10-125-B	50 Hz	12-bit resolution, 0.08 deg accuracy
Airspeed sensor	MPX7002DP	50 Hz	Typ. Pressure accuracy ± 1.6 Pa

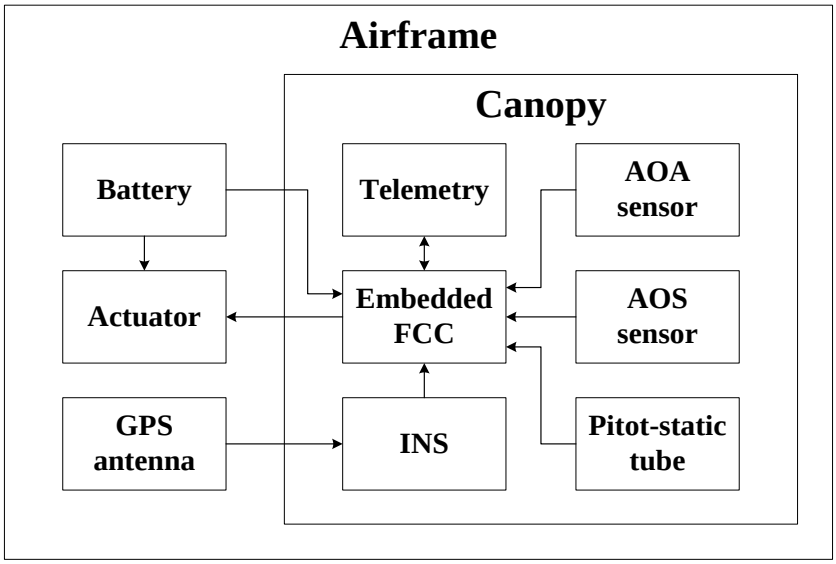

Figure 2.6: Avionics connection diagram

All of UAVs are designed to communicate and share the information with other UAVs, and therefore it is not necessary to develop a distinct ground control system (GCS) for monitoring the UAVs in formation. An extra FCC is added to the formation, for receiving the shared information and not being used

in the formation algorithm, which can function as the GCS without affecting formation guidance algorithm or formation range. In this study, three identical UAVs as shown in Fig. 2.8 and one extra FCC for ground monitoring are developed. Based on the developed avionic system, a decentralized communication system is realized.

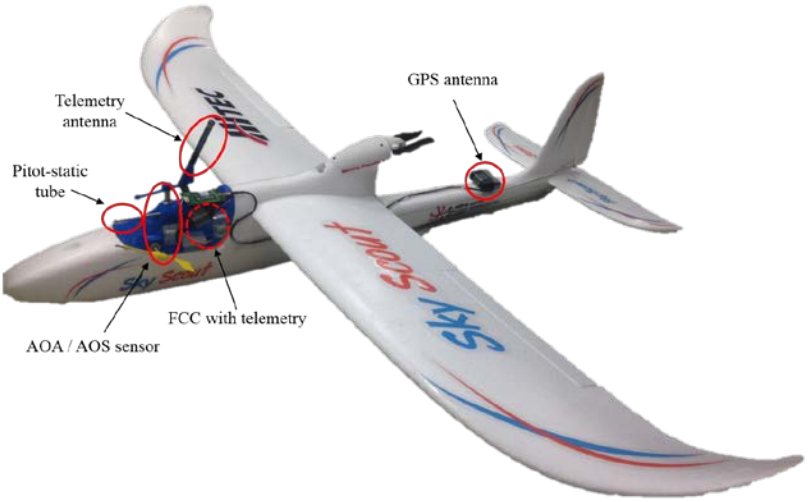

Figure 2.7: Avionics installations of the UAV

Figure 2.8: Developed three identical UAVs

2.3 Onboard Decentralized Communication

Developing information sharing technique is a challenging issue in multi-UAV operation, because unsynchronized information may cause wrong decisions by sharing incorrect sensor information among the UAVs. If all UAV communication is relayed via leader aircraft or ground control system, then the central system may become a single point of failure, which makes UAVs having a limited mission range. Therefore, decentralized communication should be realized. In the actual flight environment, communication is conducted by a wireless device, and the device should be selected considering both synchronization and decentralization. For reliable performance, standard wireless devices are considered.

Typical wireless communication devices are summarized in Table 2.4. In general, Wi-Fi is widely used for wireless communication. However, Wi-Fi requires a router to connect individual devices. Although it supports ad-hoc connection, it only connects just two system. Therefore, decentralized communication cannot be realized. Bluetooth has a relatively short communication range and only provides a connection to a single device. In contrast, ZigBee modems can communicate with multiple devices without a router and can cover a large distance. Because this protocol is designed for low power and low latency applications, it is suitable for small multiple UAV system. Therefore, the ZigBee modem is selected as the wireless device for the system.

Using the selected wireless device, i.e., the ZigBee modems, UAVs share their sensor information with each other. The sensor information to be shared includes the UAV's status such as attitude, position, velocity, and other essential parameters. Table 2.5 summarizes the communication packet used in this study, which has a 124 byte packet length and all UAVs use a same packet structure. In Table 2.5, Vel denotes a velocity, Air denotes a barometric output, and Cmd denotes a command generated from the guidance algorithm.

Table 2.4: Comparison of the wireless technology standards

	Wi-Fi	Bluetooth	ZigBee
Range	50-100 m	10-100 m	100 m-1 km
Network Topology	Point to Hub Ad-hoc	Ad-hoc	Ad-hoc, peer to peer, star, mesh
Frequency	2.4 GHz and 5 GHz	2.4 GHz	868 MHz, 900 MHz, 2.4 GHz
Complexity	High	High	Low
Power Consumption	High	Middle	Very low
Applications	Wireless LAN	Wireless device connection	Industrial monitoring Sensor network

If UAVs transmit their sensor information synchronously, data loss may occur. Multi-channel RF device can solve this problem, but it is not feasible in small UAV system.

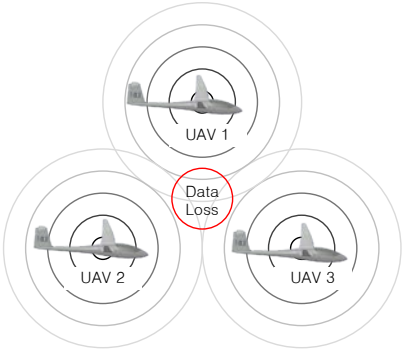

Figure 2.9: Communication failure because of simultaneous transmission

Table 2.5: Communication packets of the multiple UAVs

Data	Header	Status	Latitude	Longitude	Height	GPS time	Roll	Pitch	Yaw
Byte	1~2	3~6	7~10	11~14	15~18	19~22	23~26	27~30	31~34
format	uint16	uint16	float	float	float	uint16	float	float	float
P	Q	R	Vel N	Vel E	Vel D	Acc X	Acc Y	Acc Z	Air Height
35~38	39~42	43~46	47~50	51~54	55~58	59~62	63~66	67~70	71~74
float	float	float	float	float	float	float	float	float	float
Air speed	Gamma Cmd	Roll Cmd	Battery	Elevator	Rudder	Throttle	Aileron	Alpha	Beta
75~78	79~82	83~86	87~90	91~94	95~98	99~102	103~106	107~110	111~114
float	float	float	float	float	float	float	float	float	float
Stage	Reserved	Putter							
115~118	119~122	123~124							
float	float	uint16							

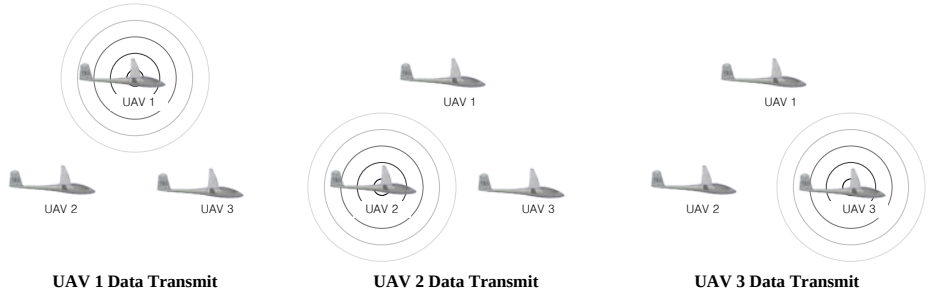

Figure 2.10. Description of the sequential cyclic communication

To achieve robust onboard sensor information sharing between UAVs, a sequential cyclic communication method is used, as shown in Fig. 2.10. The trigger UAV (UAV1) starts broadcasting its sensor information. Next, the neighboring UAV (UAV2) transmits its sensor information. This procedure continues until the last UAV (UAV3) performs a transmission. This simple concept can prevent data loss from occurring due to simultaneous data transmission. The concept of sequential cyclic communication is easily realized at a low information sharing rate (<1 Hz). However, this approach requires accurate timing control to achieve a high information sharing rate (>10 Hz), because physical communication delay may exist during data transmission. For this reason, the delay should be analyzed in detail and information sharing rate should be carefully selected to prevent information loss during communication.

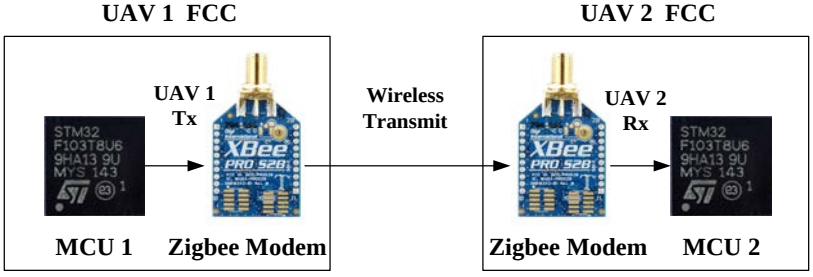

Figure 2.11. Communication flow of the two UAVs

Figure 2.11 describes a brief communication flow in the FCC, UAV1 to UAV2. Three major physical delays can be found in this communication flow. The first delay is from microprocessor 1 (MCU1) to Zigbee1, $t_{\text{MCU1 to Zigbee1}}$. If UAV1 data consist of n bytes ($8n$ bits) and the baud rate is p bps (bits per second), then the transmission delay from MCU1 to Zigbee1 can be calculated as follows

$$t_{\text{MCU1 to Zigbee1}} = \frac{8n}{p} \tag{2.1}$$

The second delay is from Zigbee1 to Zigbee2, $t_{\text{Zigbee1 to Zigbee2}}$. This delay depends on the air rate specification, that is, the RF transmission speed in air, which is inversely proportional to the carrier frequency of the modem. The data processing time inside the ZigBee modem is also included in this delay. If the ZigBee modem has an air rate of q bps, then the delay from Zigbee1 to Zigbee2 can be calculated as

$$t_{\text{Zigbee1 to Zigbee2}} = \frac{8n}{q} + t_{\text{Zigbee processing}} \tag{2.2}$$

where $t_{\text{Zigbee processing}}$ means the delay which is generated inside Zigbee modem during encoding/decoding for RF signal processing. The third delay is from Zigbee2 to MCU2, $t_{\text{Zigbee2 to MCU2}}$, which is equal to $t_{\text{MCU1 to Zigbee1}}$.

$$t_{Zigbee2\ to MCU2} = \frac{8n}{p} \tag{2.3}$$

Therefore, the communication delay can be expressed as

$$t_{\text{com\_delay}} = t_{\text{MCU1 to Zigbee1}} + t_{\text{Zigbee1 to Zigbee2}} + t_{\text{Zigbee2 to MCU2}} \tag{2.4}$$

After the first UAV1 transmission ends, the additional processing delay, $t_{\text{MCU processing}}$, is generated in UAV2 before starting second transmission by UAV2. So total transmission delay, $t_{\text{transmission}}$, can be expressed as

$$t_{\text{transmission}} = t_{\text{com\_delay}} + t_{\text{MCU processing}} \tag{2.5}$$

Equation (2.5) means that if there exists m UAVs in formation, then minimum value of information sharing period, t_{com}, is limited by $t_{\text{transmission}}$ as

$$(t_{\text{com}})_{\min} > m \times t_{\text{transmission}} \tag{2.6}$$

The considered ZigBee modem, Xbee-Pro DigiMesh900, has a baud rate of 230,400 bps and an air rate of 156,000 bps. In this case, it takes nearly 24 ms between the first transmission to the second transmission, $t_{\text{transmission}}$, for the n = 124-byte packet size case.

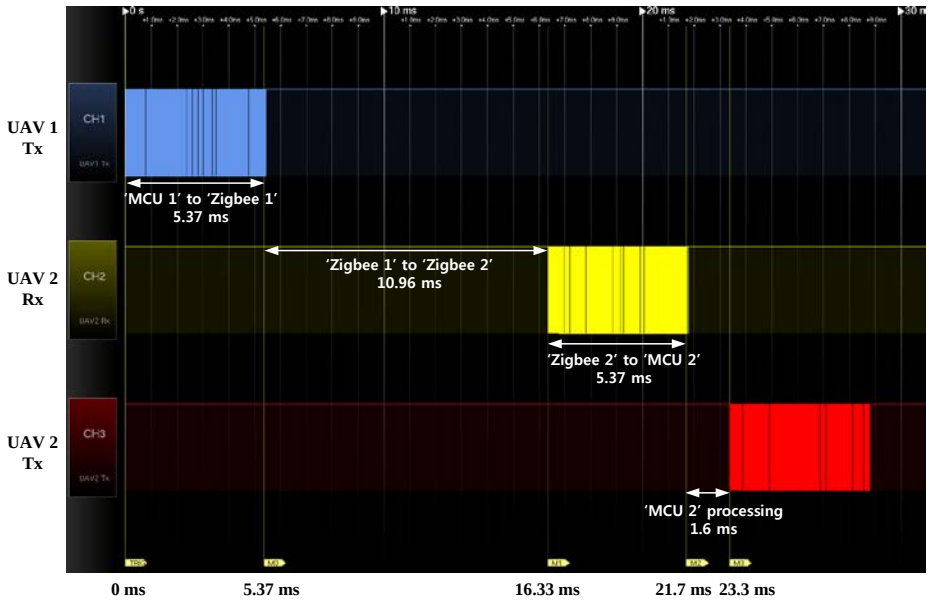

Figure 2.12: Communication delay of ZigBee between UAV1 and UAV2

The communication delays can be measured using a signal analyzer; as shown in Fig. 2.12. This experiment result shows that it actually takes 23.3 ms for transmitting UAV1's information to UAV2. The result depends on wireless device, but delays will be generated in a similar way. For four UAVs, 10 Hz of onboard sensor information sharing is possible because one cycle of four UAVs takes 24 ms × 4 = 96 ms. Accurate 10 Hz cyclic communication can be achieved if the FCC has less than 4 ms of additional delay. The typical minimum time interval of Microsoft Windows OS is in the range of 10 ms ~ 20 ms, and therefore the Windows OS is not suitable to handle the this cyclic communication. Because of the limitation, a real-time embedded FCC is used, which can control the communication timing with a 1 ms resolution.

To verify the performance of the sequential cyclic communication and to decide the communication rate, communication test is performed using three FCCs and one GCS. The GCS is used only for monitoring purpose, and it has nothing to do with the formation group. Figure 2.13 shows the configuration of sequential cyclic communication test.

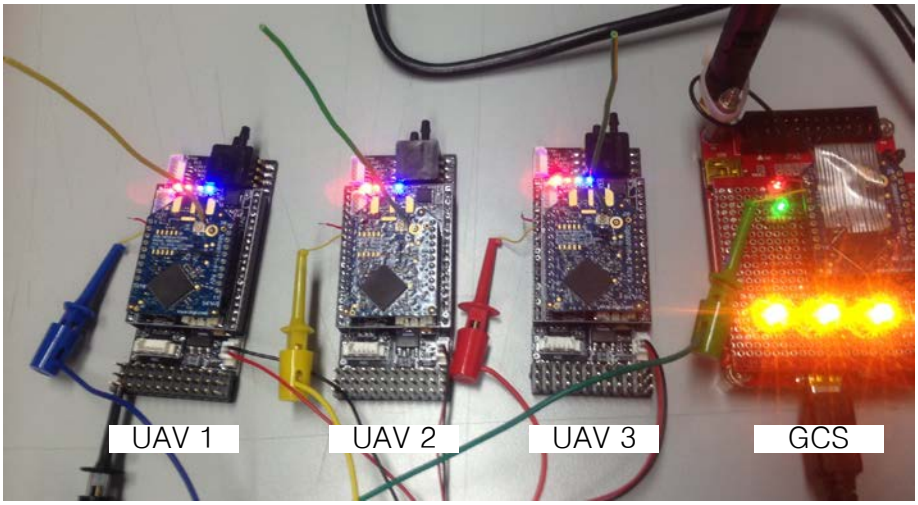

Figure 2.13: Test setup of the sequential cyclic communication

Four signal analyzer probes are connected to TX pin of each Zigbee modem to measure the transmission timing between FCCs. Sequential cyclic communication is triggered by UAV1 at 10 Hz rate, $t_{\text{com}} = 100\,\text{ms}$. When UAV1 transmits its own data to other UAVs using the ZigBee modem, other UAVs receive the data. A periodic 1 ms watching process in MCUs checks the received data, and the next UAV transmits its own data according to the given transmission order. The GCS also acts as a virtual UAV for monitoring and command uploading purposes, which does not affect the formation flight or communication structure. Communication structure is summarized in Fig. 2.14, and test result is shown in Fig. 2.15.

The result of the sequential cyclic communication shows that 10 Hz onboard sensor information sharing is properly conducted among the UAVs. It means that all UAVs know the other UAVs information in every 0.1 second without central control system relay. Finally, it can be stated that the developed communication system for the formation flight is verified.

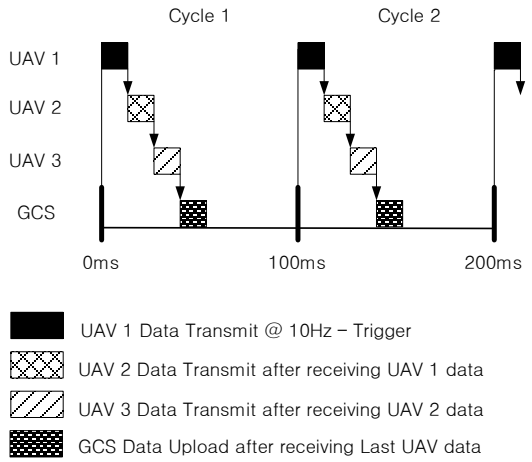

Figure 2.14: A sequential communication structure

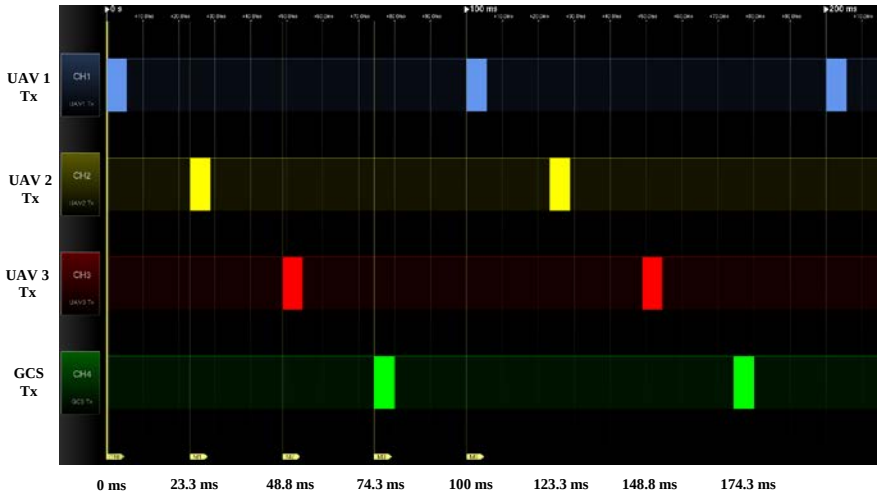

Figure 2.15: Test result of sequential cyclic communication

For safety, the periodic watching process in MCU is also monitors the communication status. If the trigger UAV is failed, communication period becomes longer than the predefined threshold, that is

$$t_{\text{com}} > kT \quad \text{where } T = 0.1s \ @10\,\text{Hz} \tag{2.7}$$

In this case, next UAV becomes the trigger UAV and the former trigger UAV is dropped from the communication group. The value of k is related to formation safety, set as $k = 8$, which allows maximum 10 m position error at 12 m/s cruse flight condition. Trigger order follows numerical order which is not related to formation structure. After developing the airframe and avionics, a system identification of UAV is conducted and a simulation environment is made to develop the guidance algorithm of the formation flight.

2.4 UAV Modeling and Simulation Setup

An accurate dynamic model of the UAV is required to design a guidance and control algorithm for multiple UAVs. A system identification flight has been conducted to obtain a linear 6-DOF dynamic model that reflects the characteristics of the fixed-wing airplane [20]. During the system identification,

Figure 2.16: Sequence of lateral system identification flight

predefined control surface inputs are used to excite the airplane dynamics, and the measurement data from the sensors are recorded. Lateral and longitudinal dynamic models are obtained by analyzing the recorded data. The lateral and longitudinal dynamics are identified separately. For aileron and rudder input, multistep 3-2-1-1 inputs are used to identify the lateral dynamics. For throttle and elevator control, multistep 3-2-1-1 inputs of the elevator and doublet input of the throttle are used to identify the longitudinal dynamics. Both identification flights are started at steady state level flight condition, and designed input sequences are automatically executed. Figure 2.16 shows lateral response of UAV during system identification flight.

Initial system matrix parameters are acquired from the flight data by least square sense, and system matrix parameters are estimated using 2-norm optimization. The lateral system model is obtained as follows

$$\begin{bmatrix} \dot{\beta} \\ \dot{\phi} \\ \dot{p} \\ \dot{r} \end{bmatrix} = \begin{bmatrix} 0.5983 & 1.0077 & 0.2074 & -1.4470 \\ 0 & 0 & 1.0000 & -0.0207 \\ -40.2283 & 0 & -8.4455 & 8.4567 \\ 9.5970 & 0 & -2.0088 & -3.9628 \end{bmatrix} \begin{bmatrix} \beta \\ \phi \\ p \\ r \end{bmatrix} + \begin{bmatrix} 0.0642 & -1.6074 \\ 0 & 0 \\ -40.1583 & 4.4587 \\ -3.6427 & -12.9649 \end{bmatrix} \begin{bmatrix} \delta_{ail} \\ \delta_{rud} \end{bmatrix} \tag{2.8}$$

The longitudinal system model is obtained as follows

$$\begin{bmatrix}\dot{V}\\ \dot{\alpha}\\ \dot{\theta}\\ \dot{q}\end{bmatrix}=\begin{bmatrix}-0.2533 & -13.163 & -9.800 & 0\\ -0.1251 & -3.0924 & 0 & 0.2288\\ 0 & 0 & 0 & 1\\ 2.6783 & 32.9942 & 0 & -15.226\end{bmatrix}\begin{bmatrix}V\\ \alpha\\ \theta\\ q\end{bmatrix} + \begin{bmatrix}0.0042 & 4.0543\\ -0.0005 & -0.5078\\ 0 & 0\\ -0.0083 & -40.9436\end{bmatrix}\begin{bmatrix}\delta_{thr}\\ \delta_{ele}\end{bmatrix} \tag{2.9}$$

Figure 2.17 and 2.18 show the lateral and longitudinal system identification results with the corresponding control inputs. System responses of the acquired model (solid line) are well matched with the recorded flight results (dashed line).

The estimated lateral and longitudinal dynamic models are implemented in a MATLAB/Simulink environment [21] to perform 6-DOF simulation as described in Fig. 2.19. Three UAVs are numerically simulated and the communication model is considered, which can control sharing rate of sensor information. The guidance and control (GNC) algorithm generates actuator commands to feedback the states of UAVs. Because the GNC algorithm is performed periodically in actual FCC, the simulation has a fixed discrete time step, t_{GNC}. In the ideal situation, GNC algorithm uses a state information generated before a single time step t_{GNC}. However, formation flight guidance requires the other UAV's state information, and therefore communication period t_{com} should be also considered. RF communication requires physical transmission time, and typical communication period t_{com} is usually longer than GNC period t_{GNC}. Therefore, the GNC algorithm uses few step ahead information of the other UAVs. This characteristics is implemented in the communication model of the simulation configuration.

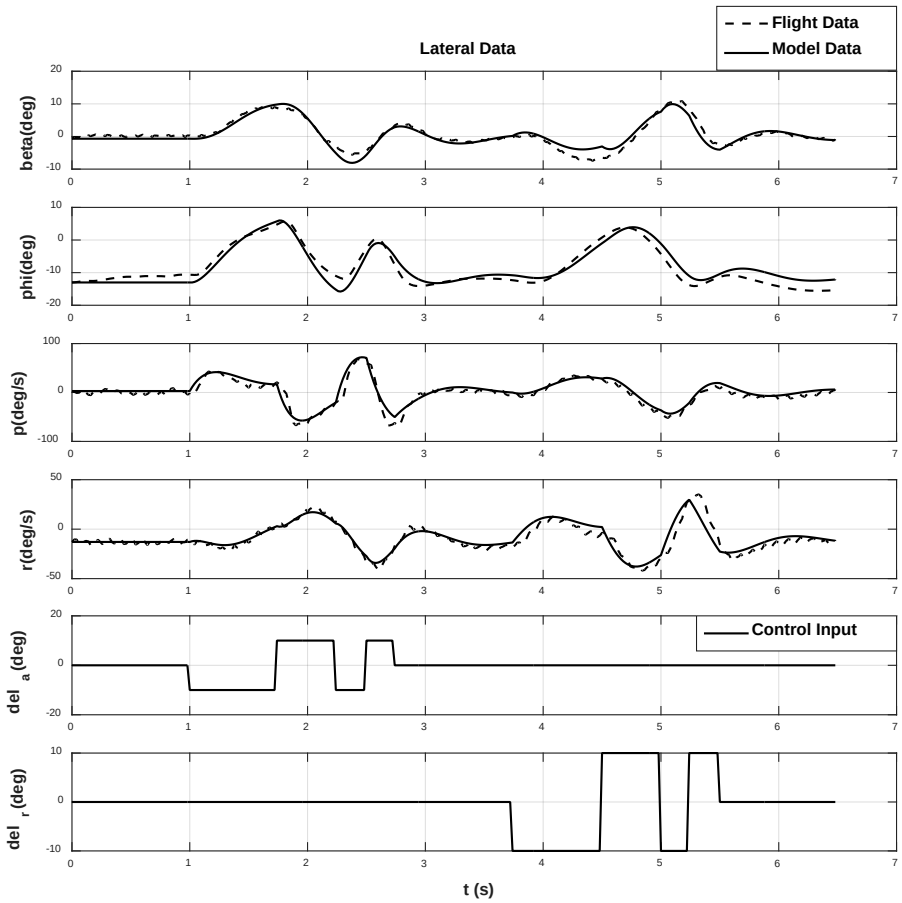

Figure 2.17: Result of the lateral system model estimation

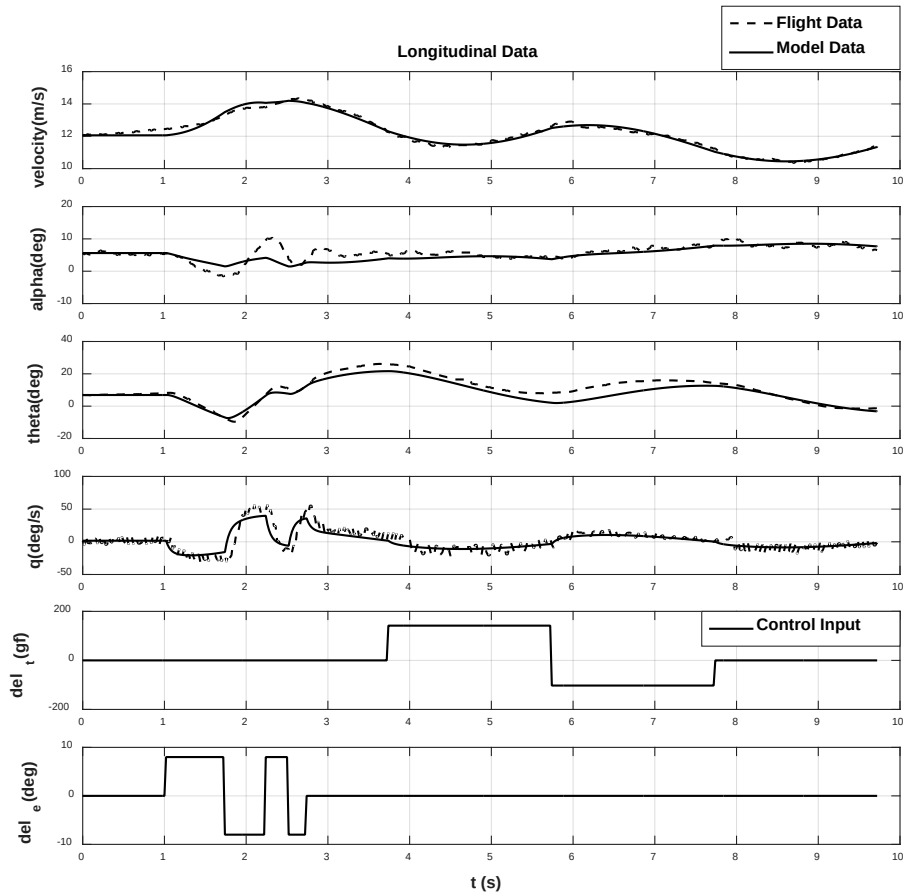

Figure 2.18: Result of the longitudinal system model estimation

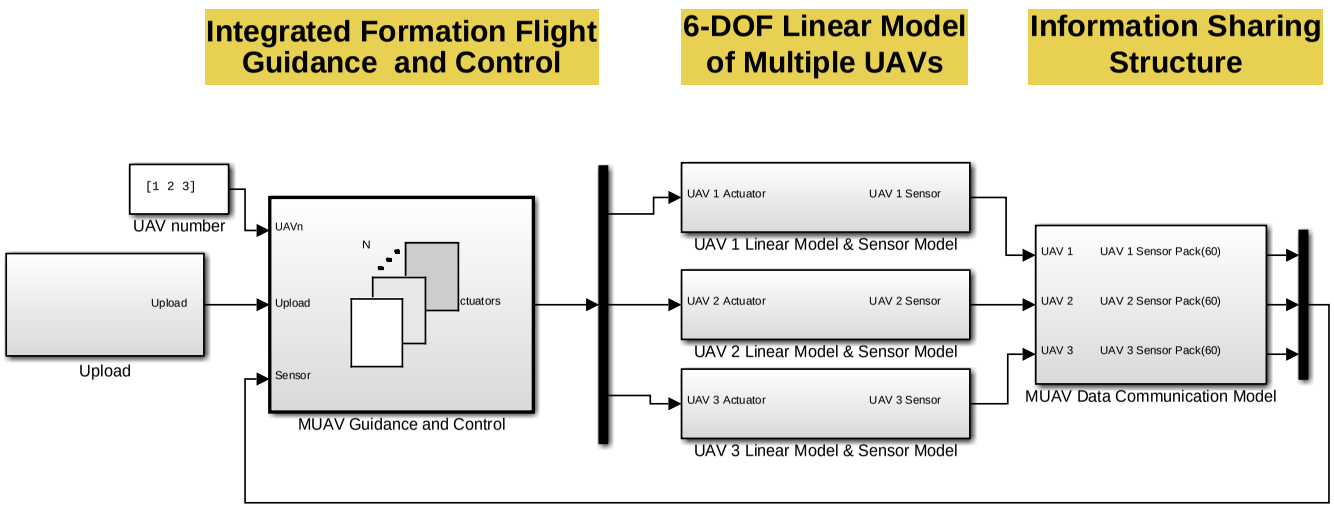

Figure 2.19: Simulation configuration of MATLAB/Simulink

3. Formation Flight Guidance

This chapter describes the formation flight guidance algorithms. Circular formation flight guidance is suitable for the omni-directional monitoring of large areas, because circular formation guidance can control the phase angles among UAVs on the circular path. On the other hand, close formation flight guidance is proper for the polygonal shape formation of fixed-wing UAVs, because such guidance can decrease the aerodynamic drag and increase survivability when flying to the next mission area.

In this chapter, circular formation guidance algorithm is first explained, and then close formation guidance algorithm is introduced. Because path-following guidance is suitable for the fixed-wing UAV guidance, both formation guidance laws are developed based on nonlinear path-following guidance [22]. Usually, horizontal motion causes a great influence on the formation flight of UAV rather than vertical motion. Therefore, in this study, formation guidance is focused on two-dimensional motion of multiple UAVs.

3.1 Circular Formation Flight Guidance

When a fixed-wing UAV monitors an area, a loitering flight is typically performed. If multiple UAVs are monitoring the area, the phase angles between UAVs should be controlled to ensure efficient area surveillance on the circular path. Nonlinear path-following guidance [23], [24] was proposed to make UAVs fly on a circular path, assuming that all UAVs are moving on a two-dimensional surface, i.e., flying at the same altitude. The stability of nonlinear path-following guidance was proven using the Lyapunov stability theorem [22] , and therefore, all UAVs asymptotically converge to the predefined path. The lateral guidance geometry of the nonlinear path following is shown in Fig. 3.1, where V is the airspeed, L is the constant guidance distance, and η is the angle between V and L.

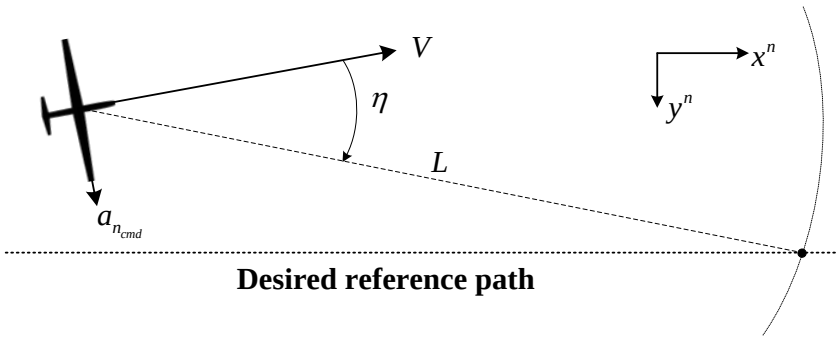

Figure 3.1: The nonlinear path-following guidance algorithm

In the lateral guidance law, by using a geometrical relationship of a velocity vector and a desired flight path, a lateral acceleration command $a_{n_{cmd}}$ can be calculated as follows

$$a_{n_{cmd}} = \frac{2V^2}{L}\sin\eta \tag{3.1}$$

To make the UAV follow the acceleration command $a_{n_{cmd}}$, a roll command ϕ_{cmd} can be used assuming that the UAV performs a coordinated turn with a centripetal acceleration a_{cen}.

$$\phi_{cmd} = \tan^{-1}\left(\frac{a_{n_{cmd}}}{g}\right) \quad \text{where} \quad a_{n_{cmd}} = a_{cen} \tag{3.2}$$

where g is the acceleration of gravity. The relationship between lateral acceleration and centripetal acceleration is described in Fig. 3.2. There is an assumption that sideslip motion is not exist. Practically, it can be canceled by AOS feedback controller, and therefore it is supposed that a coordinated flight is conducted in this study.

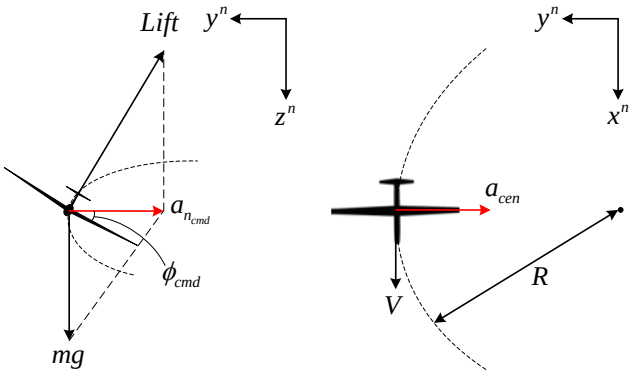

Figure 3.2: Lateral acceleration relationship

For simplicity, a position value of z-axis is omitted during formulation. A circular path can be generated from the target point $p_c^n = (p_{cx}, p_{cy})$ and the loitering radius R, as shown in Fig. 3.3. $p_1^n = (p_{x1}, p_{y1})$ denotes the position of 1st UAV, $p_2^n = (p_{x2}, p_{y2})$ denotes the position of 2nd UAV, and $\hat{p}_2^n = (\hat{p}_{x2}, \hat{p}_{y2})$ denotes the desired position of 2nd UAV. It is assumed that the 1st UAV located ahead of 2nd UAV. The target point p_c^n is assumed to be the origin $(0,0)$ without loss of generality.

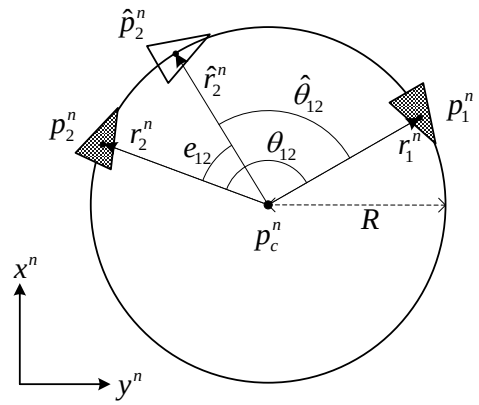

Figure 3.3: Phase angles on the circular path

Once the UAVs are flying on the circular path using the nonlinear path following guidance, a phase angle can be maintained by controlling the airspeed of the UAV. The relative phase angles of the UAVs are calculated between UAVs. The radius vectors of the UAVs are calculated using the positions of the UAVs and the target position as

$$r_i^n = p_i^n - p_c^n \text{ where } i = 1 \cdots m \tag{3.3}$$

where the number of UAVs in circular path is *m*. The phase angles of the UAVs are calculated as

$$\theta_{12} = \cos^{-1}\left(\frac{r_1^n \bullet r_2^n}{\left\| r_1^n \right\| \left\| r_2^n \right\|} \right) \tag{3.4}$$

Note that the phase angle has a positive value in the range of $[0, \pi]$. The target phase angle $\hat{\theta}_{12}$ is determined by considering the number of UAVs as

$$\hat{\theta}_{12} = 2\pi / m, \; m \geq 2 \tag{3.5}$$

Using the phase angle θ_{12} and target phase angle $\hat{\theta}_{12}$, the phase angle error e_{12} can be calculated as follows

$$e_{12} = \hat{\theta}_{12} - \theta_{12} \tag{3.6}$$

A speed command for controlling the phase angle can be generated using the phase angle error as

$$V_{cmd} = V_{cruise} + K_v e_{12}, \quad K_v < 0 \tag{3.7}$$

where V_{cruise} is the cruise velocity during level flight, and K_v is a proportional velocity guidance gain. To prevent each UAV from entering a stall speed, a range of velocity command V_{cmd} has a saturation value.

The flight path angle command, γ_{cmd}, is generated to track the target height h_{ref} as follows

$$\begin{aligned} h_{err} &= h_{ref} - h \\ \gamma_{cmd} &= K_p h_{err} + K_i \int h_{err} dt + K_d \dot{h}_{err} \end{aligned} \tag{3.8}$$

where K_p, K_i, K_d are the proportional, integral, and derivative gains of the height controller, respectively. The reference altitude can be set depending on mission status.

Generated guidance angle commands are designed to the longitudinal and lateral controllers. The roll command ϕ_{cmd} are controlled by the lateral controller as shown in Fig. 3.4. The flight path angle command γ_{cmd} and the velocity command V_{cmd} are controlled by the longitudinal controller as shown in Fig. 3.5. These lateral and longitudinal controllers are used throughout the dissertation.

The developed circular formation flight guidance is verified by numerical simulation. Three UAVs are circling around the origin point with equal phase angle. During circular formation flight, UAV first enters into the predefined circular path, and then, phase angle controller regulates the phase angles between the UAVs depending on the number of UAVs in the circular path. Simulation parameters are summarized in Table 3.1, and the circular formation flight result is shown in Fig. 3.6. It is shown that phase angles between UAV are converged to the target phase angle.

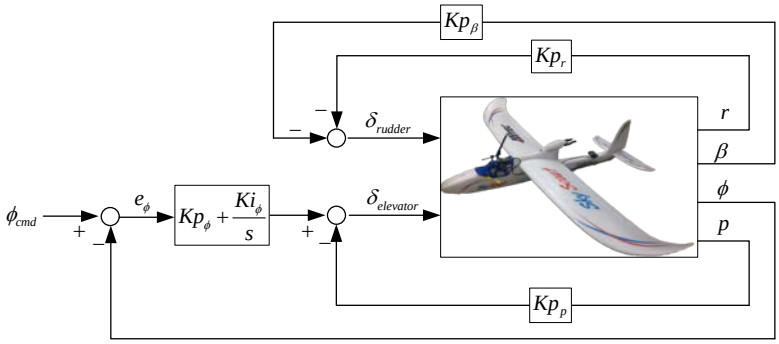

Figure 3.4: Description of lateral controller

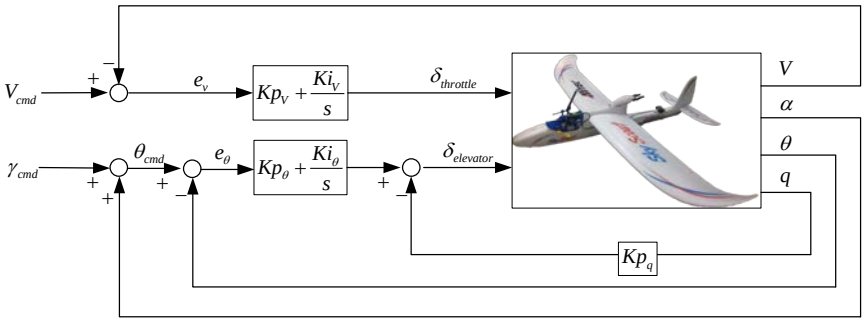

Figure 3.5: Description of longitudinal controller

Table 3.1: Initial simulation parameters of the circular formation guidance

Parameter	Value	Parameter	Value
$(p_1^n)_{initial}$	(-130,0,60)	$(\psi_1)_{initial}$	0 deg
$(p_2^n)_{initial}$	(-130,100,60)	$(\psi_1)_{initial}$	0 deg
$(p_3^n)_{initial}$	(-130,-100,60)	$(\psi_1)_{initial}$	0 deg
$(V_1^b)_{inital}$	11 m/s	t_{simul}	0.02 s
$(V_2^b)_{inital}$	11 m/s	t_{GNC}	0.02 s
$(V_3^b)_{inital}$	11 m/s	t_{com}	0.02 s

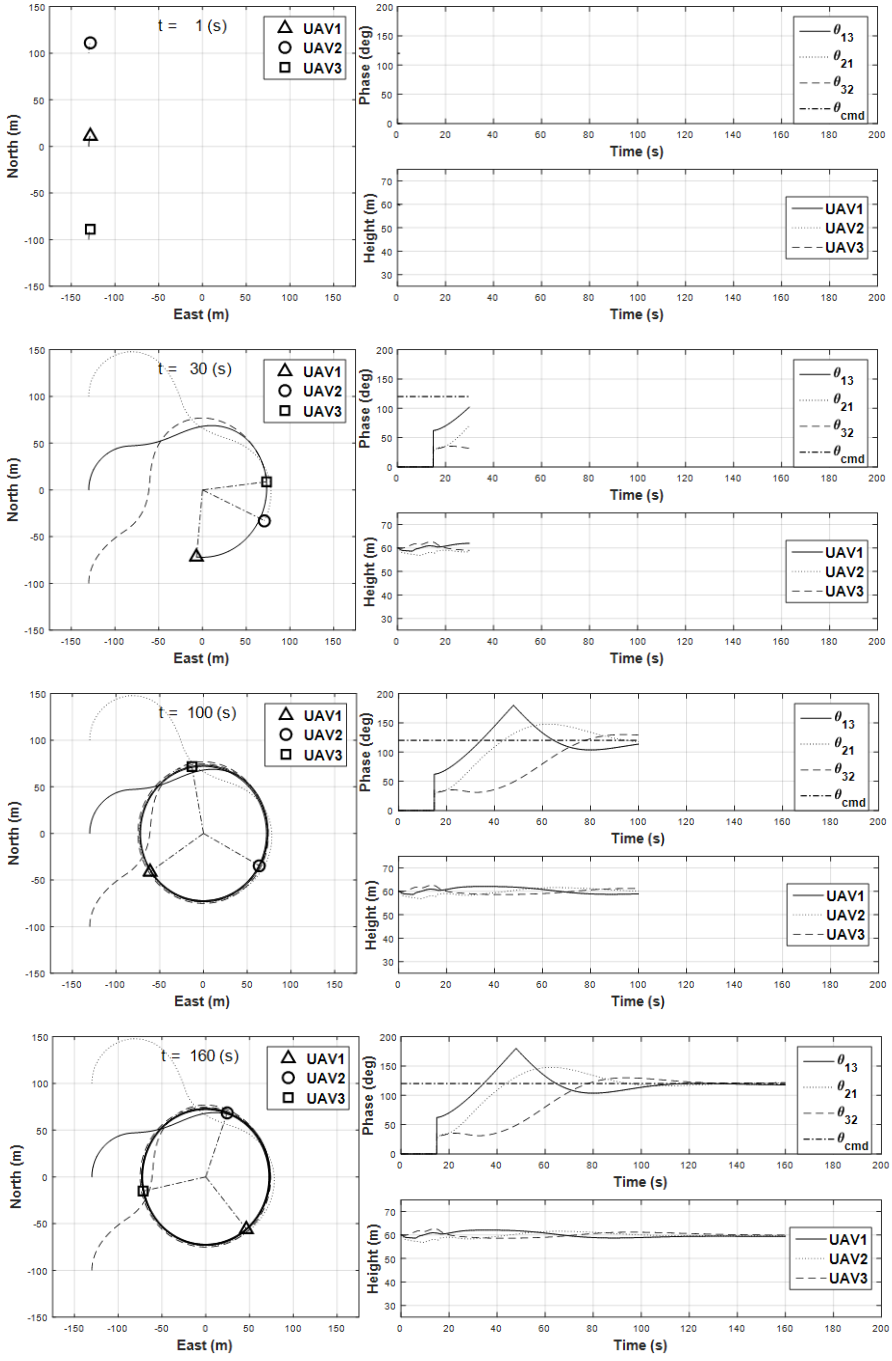

Figure 3.6: Simulation results of the circular formation guidance

3.2 Close Formation Flight Guidance

For close formation flight the separated longitudinal and lateral guidance laws are designed to increase the performance of the formation flight, because fixed-wing airplanes have different flight characteristics in the longitudinal and lateral axes. The lateral guidance law of the close formation flight is designed based on the nonlinear path-following guidance, as shown in Fig. 3.1.

Two close formation flight algorithms, behavioral and leader-follower, are designed, and the performances of both algorithms are verified by numerical simulation.

3.2.1 Behavioral Approach based Formation Flight Guidance

The formation geometric center (FGC) method, a typical expression of behavioral approach, requires the FGC point and the formation heading direction to determine the formation position of each UAV. The FGC and heading direction are determined from the state of UAVs in formation. While keeping the formation geometry, the FGC should be guided to following the target path for formation movement. To make problem simple, formation keeping and formation movement are separately explained.

Figure 3.7 shows formation keeping algorithm in FGC guidance. In Fig. 3.7, (x_{FGC}^b, y_{FGC}^b) denotes the body frame of the FGC aligned with V_{FGC}^n, $p_i^n = (p_{ix}^n, p_{iy}^n)$ denotes the *i*-th UAV's inertial position, $\hat{p}_i^n = (\hat{p}_{ix}^n, \hat{p}_{iy}^n)$ denotes the target formation position of the *i*-th UAV. Once *i*-th UAV's formation path and guidance point $p_{L_i}^n$ are determined, UAV can generate a formation acceleration command a_{n_i}.

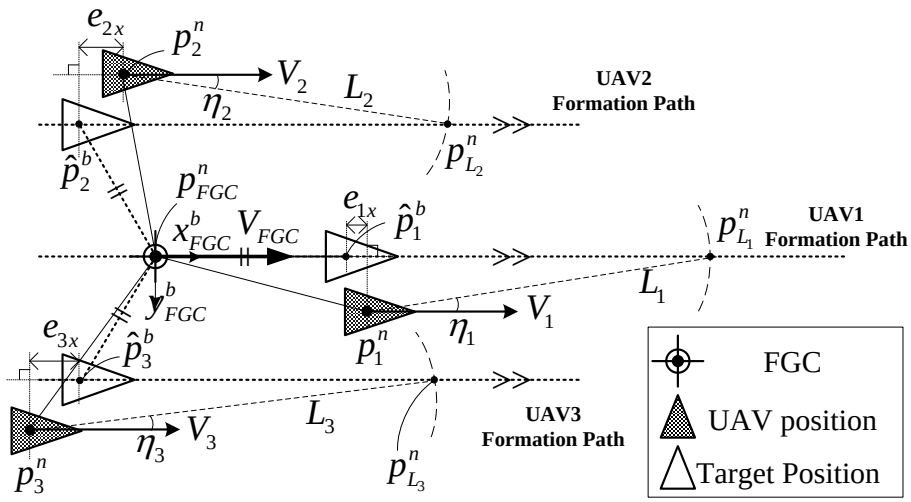

Figure 3.7: Suggested FGC guidance: formation keeping

The FGC is calculated by sum of each UAV's position as

$$p_{FGC}^n = \sum_{i=1}^{m} \frac{p_i^n}{m} \text{ where } i = 1 \cdots m \tag{3.9}$$

where *m* denotes the number of UAVs in formation. The heading angle of the FGC, ψ_{FGC}, is an average value of the heading angle of individual UAV as

$$\psi_{FGC} = \sum_{i=1}^{m} \frac{\psi_i}{m} \tag{3.10}$$

The velocity of the FGC, V_{FGC}, are calculated as follows

$$V_{FGC} = \sum_{i=1}^{m} \frac{V_i}{m} \tag{3.11}$$

Once the FGC and heading angle are calculated, target formation positions, $\hat{p}_i^n = (\hat{p}_{ix}, \hat{p}_{iy})$, where UAVs should be guided, can be determined. Let us consider a triangular formation shape as the target formation.

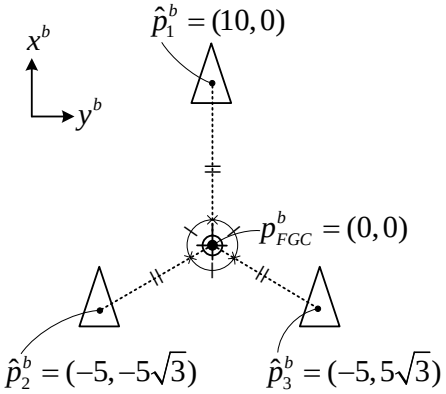

Figure 3.8: Formation geometry of the suggested FGC formation

The rotation matrix from the navigation frame to the FGC body is defined as

$$C_n^b = \begin{bmatrix} \cos\psi_{FGC} & \sin\psi_{FGC} \\ -\sin\psi_{FGC} & \cos\psi_{FGC} \end{bmatrix}, \quad C_b^n = \left(C_n^b\right)^T \tag{3.12}$$

The UAV positions are transformed to the FGC body frame as

$$p_i^b = C_n^b \left(p_i^n - p_{FGC}^n \right) \tag{3.13}$$

In the FGC body frame, formation path of the UAV is aligned to x^b axis, and therefore the guidance point $p_{L_i}^n$ can be calculated as

$$\begin{aligned} & p_{L_i}^n = C_b^n p_{L_i}^b + p_{FGC}^n \\ & \text{where } p_{L_i}^b = \begin{bmatrix} p_{L_{ix}} & p_{L_{iy}} \end{bmatrix}^T, \ \left\| p_{L_i}^b - p_i^b \right\| = L_i, \ and \ p_{L_{iy}} = \hat{p}_{yi} \end{aligned} \tag{3.14}$$

Using the geometrical relationship of the guidance point $p_{L_i}^n$, the UAV position p_i^n and V_i, the angular difference η_i can be calculated.

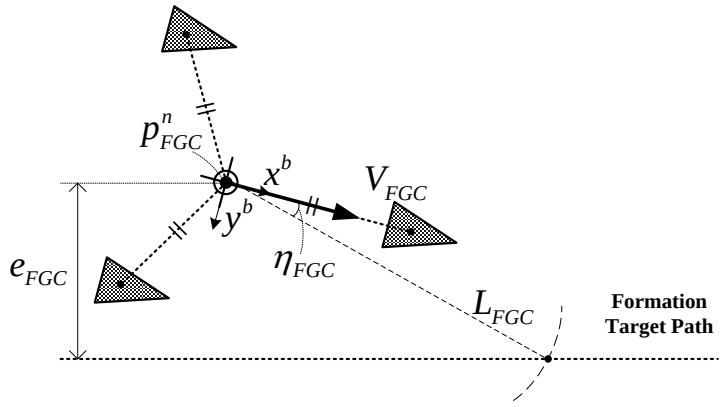

Figure 3.9: Suggested FGC guidance: formation path following

Simultaneously, the formation itself should be also guided to the target formation path as shown in Fig. 3.9. From the FGC and formation path geometry, η_{FGC} can be calculated. The parameter L_{FGC} is related with the formation dynamic. The formation path error, e_{FGC}, is formation path error between the FGC and the target formation path.

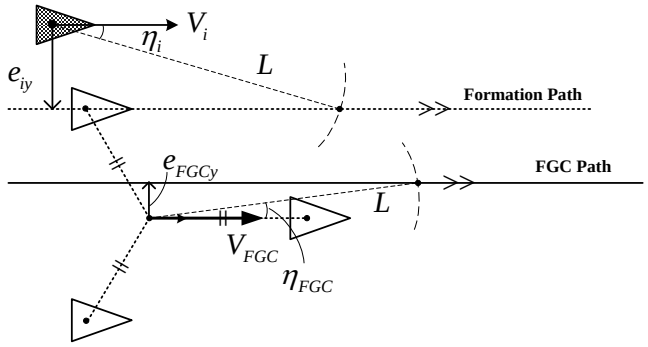

Figure 3.10: Formation keeping and path following of the suggested FGC guidance

The i-th UAV should follow a combined path satisfying both formation keeping and formation path moving as shown in Fig. 3.10. The i-th UAV should be

guided to the formation path, and the lateral path error e_{iy} is generated. Simultaneously, the FGC point should be guided to the FGC path that generates a lateral formation path error e_{FGCy}. By adding these path errors, a combined path error e_{Fused} can be calculated.

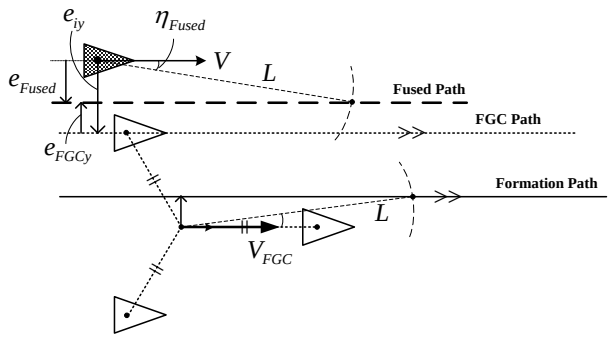

Figure 3.11: Description of the combined path of *i*-th UAV

Figure 3.11 shows the brief description of the suggested FGC guidance algorithm. If η_i and η_{FGC} are small, then angular differences can be expressed as

$$\begin{aligned} \eta_i &\approx \sin(\eta_i) = \frac{e_{iy}}{L} \\ \eta_{FGC} &\approx \sin(\eta_{FGC}) = \frac{e_{FGCy}}{L} \end{aligned} \tag{3.15}$$

The combined angular difference η_{Fused} can be expressed as

$$\begin{aligned} \eta_{Fused} &\approx \sin(\eta_{Fused}) = \frac{e_{Fused}}{L} = \frac{e_{iy}}{L} + \frac{e_{FGCy}}{L} \\ &\approx \eta_i + \eta_{FGC} \end{aligned} \tag{3.16}$$

Consequently, a lateral acceleration command of the i-th UAV, a_{n_i}, can be calculated as

$$a_{n_i} = \frac{2(V_i)^2}{L}\sin(\eta_i + \eta_{FGC}) \quad \text{where } i = 1 \cdots m \tag{3.17}$$

A roll command is used to follow the generated acceleration command as

$$\phi_{cmd_i} = \tan^{-1}\left(\frac{a_{n_i}}{g}\right) \tag{3.18}$$

A longitudinal position is controlled using the longitudinal formation error. The formation position error, $\hat{e}_i^b$, is defined as

$$e_i^b = \begin{bmatrix} e_{ix} \\ e_{iy} \end{bmatrix} = p_i^b - \hat{p}_i^b \tag{3.19}$$

A speed command for controlling longitudinal position is generated as

$$V_{cmd_i} = V_{cruise} + K_v e_{ix} \quad \text{where } K_v < 0,\ i = 1 \cdots m \tag{3.20}$$

To verify the proposed formation guidance algorithm, numerical simulation is performed. Three UAVs are considered for the close formation using the proposed FGC guidance to follow the round-shaped square path. Formation position errors are calculated to identify the formation keeping performance. Initial conditions and simulation parameters are summarized in Table 3.2.

Numerical simulation is performed with a simulation period t_{simul}, and GNC algorithm is performed at with a period of t_{GNC}. Communication period t_{com} is set as same as t_{GNC}, and therefore performance in the ideal case is tested.

Table 3.2: Initial simulation parameters (the suggested FGC method @ t_{com} = 0.02 s)

Parameter	Value	Parameter	Value
$(p_1^n)_{initial}$	(-200,-100,60)	$(\psi_2)_{initial}$	0 deg
$(p_2^n)_{initial}$	(-240,-130,60)	$(\psi_3)_{initial}$	0 deg
$(p_3^n)_{initial}$	(-180,-130,60)	$L_{1\cdots3}$	30
$(V_1)_{inital}$	11 m/s	L_{FGC}	30
$(V_2)_{inital}$	11 m/s	t_{simul}	0.02 s
$(V_3)_{inital}$	11 m/s	t_{GNC}	0.02 s
$(\psi_1)_{initial}$	0 deg	t_{com}	0.02 s

Figure 3.12 shows the trajectory result of the proposed FGC algorithm, and Fig. 3.13 shows the formation position result. In Fig. 3.13, it is shown that each UAV keeps the target position, and the close formation flight is conducted well. Performance of formation geometry keeping is shown in Fig. 3.14. Position errors increases when the formation follows the curved path, but the FGC follows the target trajectory well. Since the main objective of the FGC method is to maintain the FGC, there exist overlapped flight trajectories as shown in Fig. 3.12, because the FGC algorithm does not directly reflect the individual flight path of each UAV.

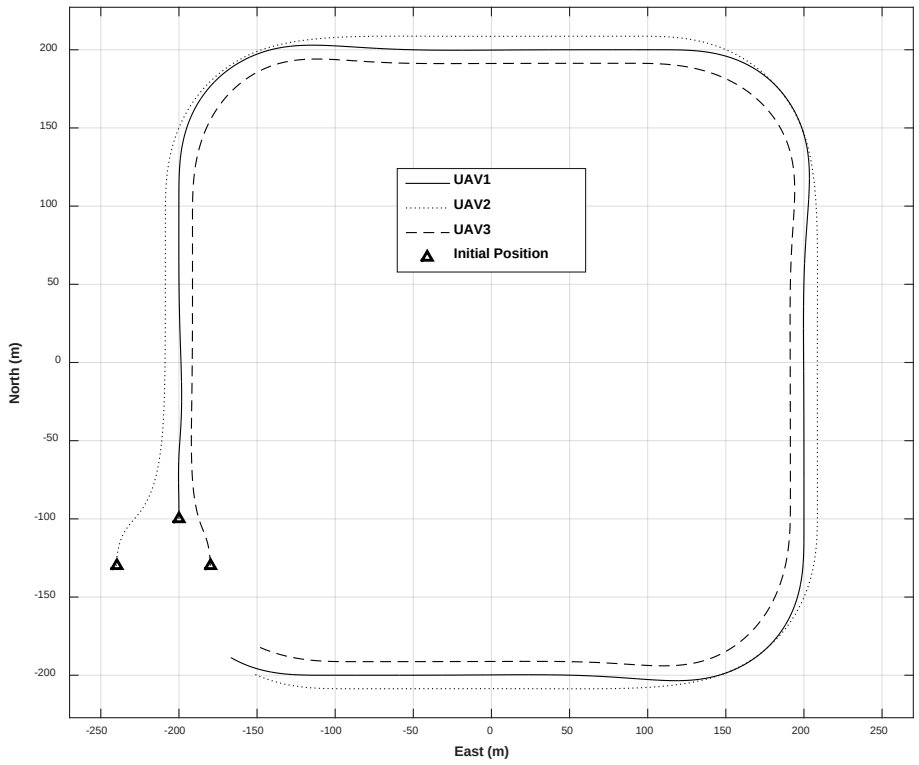

Figure 3.12: Simulation results of the suggested FGC formation algorithm (trajectories of UAVs @ t_{com} = 0.02 s)

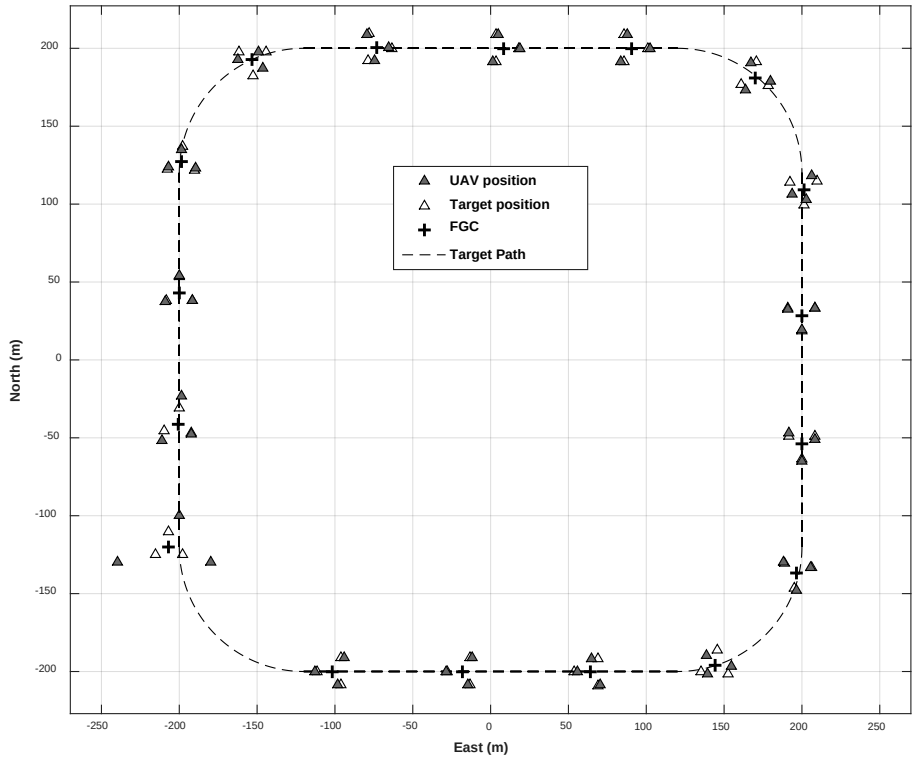

Figure 3.13: Simulation results of the suggested FGC formation algorithm (formation positions @ t_{com} = 0.02 s)

.

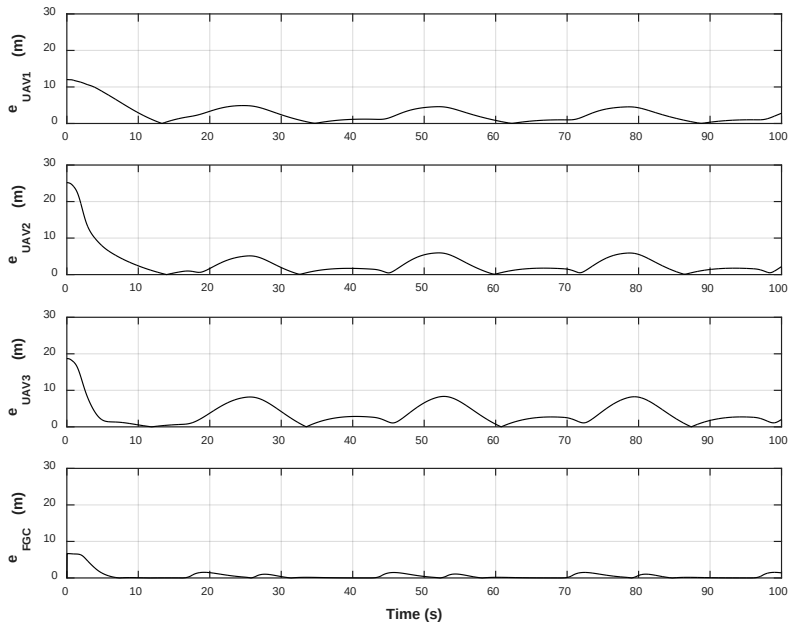

Figure 3.14 Simulation results of the suggested FGC formation algorithm (formation position errors @ t_{com} =0.02 s)

To investigate the effect of communication period, t_{com} =1 s case is considered. Simulation parameters are summarized in Table 3.3. Figure 3.15 shows the trajectory result, and Fig. 3.16 shows the formation position result. Formation position errors are shown in Fig. 3.17. When there exists large communication delay in the FGC algorithm, calculation of the FGC point becomes inaccurate, because it is calculated based on the previous position of other UAVs. This makes the UAV follow wrong target position, and it may cause a recursive position error of the FGC.

Table 3.3: Initial simulation parameters (the suggested FGC method @ t_{com} = 1.00 s)

Parameter	Value	Parameter	Value
$(p_1^n)_{initial}$	(-200,-100,60)	$(\psi_2)_{initial}$	0 deg
$(p_2^n)_{initial}$	(-240,-130,60)	$(\psi_3)_{initial}$	0 deg
$(p_3^n)_{initial}$	(-180,-130,60)	$L_{1\cdots3}$	30
$(V_1)_{inital}$	11 m/s	L_{FGC}	30
$(V_2)_{inital}$	11 m/s	t_{simul}	0.02 s
$(V_3)_{inital}$	11 m/s	t_{GNC}	0.02 s
$(\psi_1)_{initial}$	0 deg	t_{com}	1.00 s

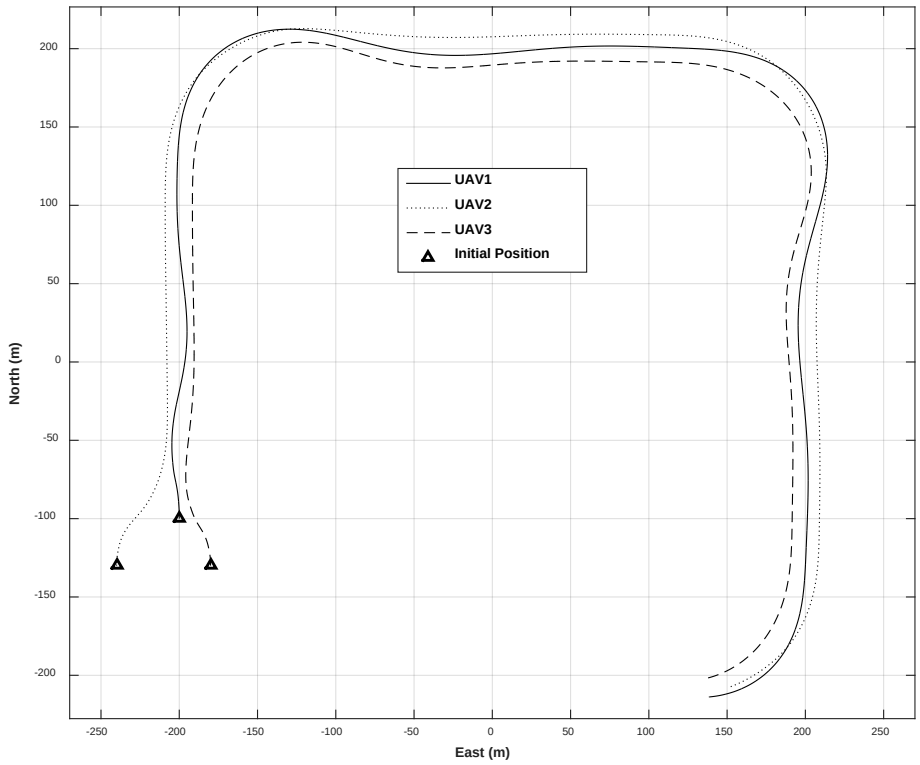

Figure 3.15: Simulation results of the suggested FGC formation algorithm (trajectories of UAVs @ t_{com} = 1.00 s)

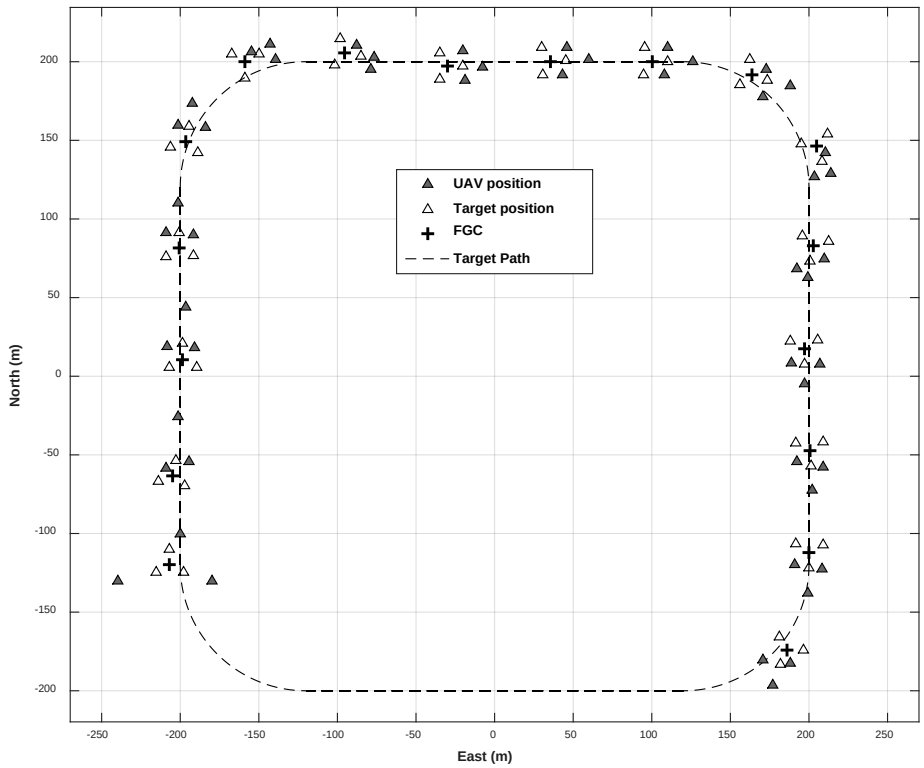

Figure 3.16: Simulation results of the suggested FGC formation algorithm (formation positions @ t_{com} = 1.00 s)

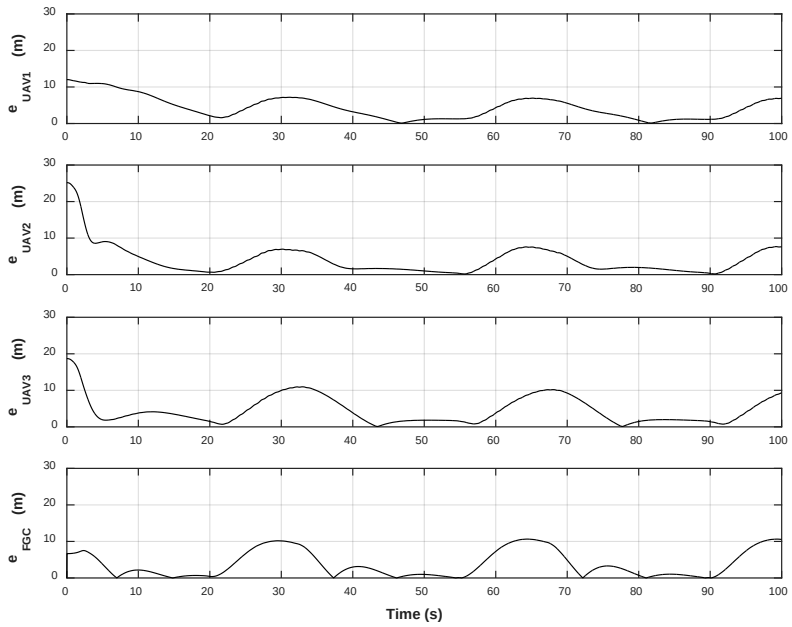

Figure 3.17: Simulation results of the suggested FGC formation algorithm (formation position errors @ t_{com} = 1.00 s)

3.2.2 **Leader-Follower Approach based Formation Flight Guidance**

In the leader-follower formation flight, the leader UAV follows the prescribed target path, and it shares all of the sensor information with the followers. The follower UAVs estimate the leader's path based on the most recent position data of the leader UAV. Using the estimated path of the leader UAV, the follower UAVs generate their own flight paths using the formation guidance law. By estimating the leader's flight path, the leader-follower formation guidance is transformed to the path-following problem. Figure 3.18 shows a geometric description of the path estimation process.

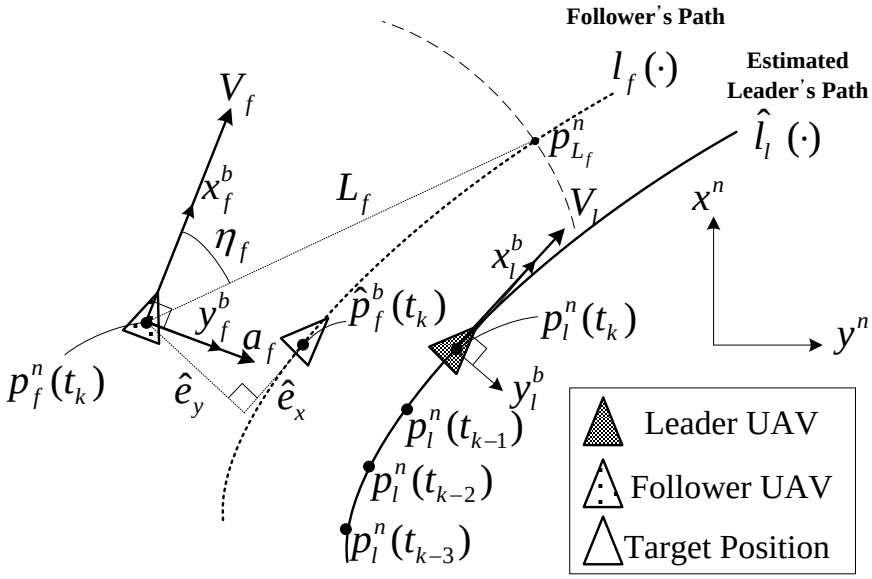

Figure 3.18. Suggested formation path generation algorithm of the follower UAV

In Fig. 3.18, (x^n, y^n) denotes an inertial navigation frame, (x_l^b, y_l^b) denotes the body-fixed frame of the leader UAV, (x_f^b, y_f^b) denotes the body-fixed frame of the follower UAV, $\hat{p}_f^b = (\hat{p}_{fx}, \hat{p}_{fy})$ denotes the target position

of the follower UAV. The subsequent position data of the leader UAV, $p_l^n(t_k)$, are recorded by the follower UAV to estimate the leader's flight trajectory.

$$p_l^n(t_k) = \begin{bmatrix} p_{lx}(t_k) \\ p_{ly}(t_k) \end{bmatrix},\ t_k = t_0 + kt_{com},\ k = 0,1,2,3 \tag{3.21}$$

The recoded positions depend on a communication interval t_{com}. To estimate the leader's path, the leader's previous positions are subtracted from the current leader's position $p_l^n(t_k)$ as

$$\begin{aligned} \Delta p_l^n(t_k) &= 0 \\ \Delta p_l^n(t_{k-1}) &= p_l^n(t_{k-1}) - p_l^n(t_k) \\ \Delta p_l^n(t_{k-2}) &= p_l^n(t_{k-2}) - p_l^n(t_k) \\ \Delta p_l^n(t_{k-3}) &= p_l^n(t_{k-3}) - p_l^n(t_k) \end{aligned} \tag{3.22}$$

The relative positions, Δp_l^n, are rotated to the body frame using the leader's heading angle $\psi_l(k)$ as

$$\Delta p_l^b = C_n^b \times \Delta p_l^n,\ C_n^b = \begin{bmatrix} \cos(\psi_l(k)) & \sin(\psi_l(k)) \\ -\sin(\psi_l(k)) & \cos(\psi_l(k)) \end{bmatrix} \tag{3.23}$$

The follower's position is also transformed to the body frame as

$$\Delta p_f^b = C_n^b \times \Delta p_f^n,\ \Delta p_f^n = p_f^n(t_k) - p_l^n(t_k) \tag{3.24}$$

Using the relative position $\Delta p_l^b(t_k) = \begin{bmatrix} \Delta p_{lx}(t_k) & \Delta p_{ly}(t_k) \end{bmatrix}^T$, the coefficients of the cubic polynomial function $\begin{bmatrix} c_{11} & c_{21} & c_{31} & c_{41} \end{bmatrix}^T$ can be calculated using the least squares method.

$$\begin{bmatrix} c_{11} \\ c_{21} \\ c_{31} \\ c_{41} \end{bmatrix} = (A^T A)^{-1} A^T Y \tag{3.25}$$

where $Y = \begin{bmatrix} \Delta p_{ly}(t_k) \\ \Delta p_{ly}(t_{k-1}) \\ \Delta p_{ly}(t_{k-2}) \\ \Delta p_{ly}(t_{k-3}) \end{bmatrix}, A = \begin{bmatrix} (\Delta p_{lx}(t_k))^3 & (\Delta p_{lx}(t_k))^2 & \Delta p_{lx}(t_k) & 1 \\ (\Delta p_{lx}(t_{k-1}))^3 & (\Delta p_{lx}(t_{k-1}))^2 & \Delta p_{lx}(t_{k-1}) & 1 \\ (\Delta p_{lx}(t_{k-2}))^3 & (\Delta p_{lx}(t_{k-2}))^2 & \Delta p_{lx}(t_{k-2}) & 1 \\ (\Delta p_{lx}(t_{k-3}))^3 & (\Delta p_{lx}(t_{k-3}))^2 & \Delta p_{lx}(t_{k-3}) & 1 \end{bmatrix}$

The polynomial path function of the leader UAV can be estimated in terms of the leader's body frame as

$$\hat{l}_l(x) = c_{11}x^3 + c_{21}x^2 + c_{31}x + c_{41} \tag{3.26}$$

Based on the estimated polynomial path function $\hat{l}_l(x)$, the follower UAV generates a formation path $l_f(x)$ with the lateral distance $\hat{p}_{fy}$ aligned with the x_l^b axis as

$$l_f(x) = \hat{l}_l(x) + \hat{p}_{fy} \tag{3.27}$$

The guidance point $p_{L_f}^n$ can be calculated as

$$p_{L_f}^n = C_b^n p_{L_f}^b + p_l^n(k) \tag{3.28}$$

where $p_{L_f}^b = \begin{bmatrix} p_{L_f x} & p_{L_f y} \end{bmatrix}^T$, $\left\| p_{L_f}^b - \Delta p_f^b \right\| = L_f$, and $p_{L_f y} = l_f(p_{L_f x})$

The follower UAV can follow the generated formation path by applying the nonlinear path-following guidance law. A roll angle ϕ_{cmd} command is calculated using the lateral acceleration command a_f as

$$\phi_{cmd} = \tan^{-1}\left(\frac{a_f}{g}\right) \text{ where } a_f = \frac{2V_f^{\,2}}{L_f}\sin\eta_f \tag{3.29}$$

Finally, the attitude controller makes the UAV follow the roll angle command ϕ_{cmd}. Formation position error is calculated as

$$e_f^b = \begin{bmatrix} e_{fx} \\ e_{fy} \end{bmatrix} = \Delta p_f^b - \hat{p}_f^b \tag{3.30}$$

Once the follower UAV is on the formation path, a longitudinal velocity command V_{ref} is generated to control the longitudinal formation position error $\hat{e}_{fx}$ aligned to the x_f^b-axis as

$$V_{cmd} = V_{cruise} + K_d e_{fx} \text{ where } K_d < 0 \tag{3.31}$$

To verify the proposed leader-follower guidance algorithm, numerical simulation is conducted. To compare with FGC algorithm, same simulation condition and formation geometry are used. UAV1 is set as the leader UAV. UAV2 is set as the left wing, which has a formation position $\hat{p}_{f1}^b = (-15m, -5\sqrt{3}\,m)$. And UAV3 is set as the right wing, which has a formation position $\hat{p}_{f2}^b = (-15m, 5\sqrt{3}\,m)$. Figure 3.19 shows the formation geometry.

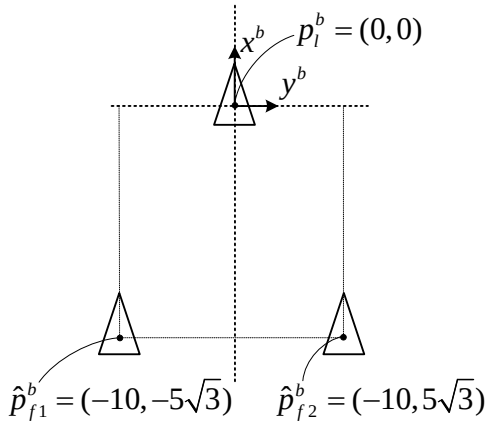

Figure 3.19: Formation geometry of the leader-follower formation

Table 3.4 shows the initial conditions of the simulation. Figure 3.20 shows the trajectory result of the proposed leader-follower algorithm and Fig. 3.21 shows the formation position result. As shown in Fig. 3.20, flight trajectories of UAVs form a parallel trajectory, because the proposed leader-follower algorithms is based on the trajectory of distinct reference, the leader UAV.

Table 3.4: Initial simulation parameters (the suggested Leader- follower method @ t_{com} = 0.02 s)

Parameter	Value	Parameter	Value
$(p_1^n)_{initial}$	(-200,-100,60)	$(\psi_1)_{initial}$	0 deg
$(p_2^n)_{initial}$	(-240,-130,60)	$(\psi_2)_{initial}$	0 deg
$(p_3^n)_{initial}$	(-180,-130,60)	$(\psi_3)_{initial}$	0 deg
$(V_1)_{inital}$	11 m/s	t_{simul}	0.02 s
$(V_2)_{inital}$	11 m/s	t_{GNC}	0.02 s
$(V_3)_{inital}$	11 m/s	t_{com}	0.02 s

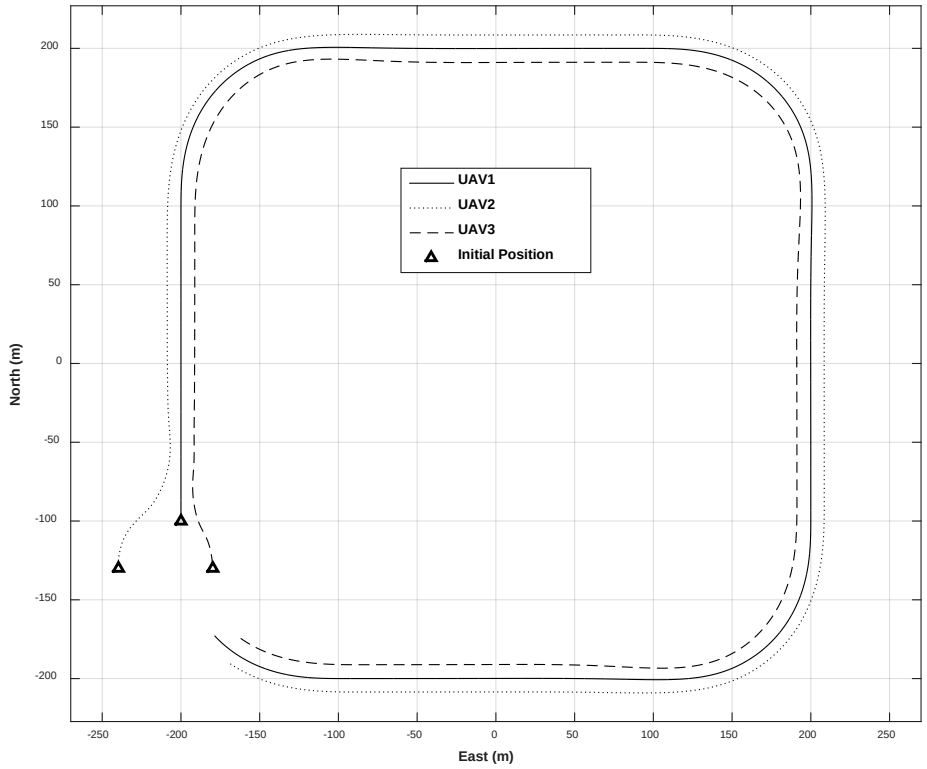

Figure 3.20: Simulation results of the suggested leader-follower formation algorithm (trajectories of UAVs @ t_{com} = 0.02 s)

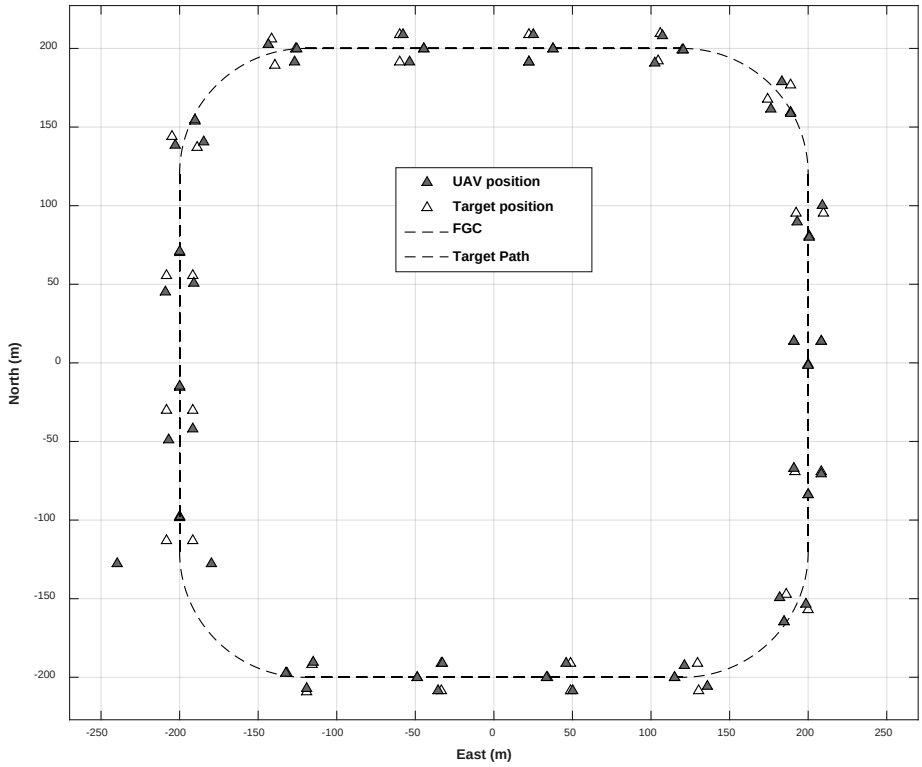

Figure 3.21: Simulation results of the suggested leader-follower formation algorithm (formations positions @ t_{com} = 0.02 s)

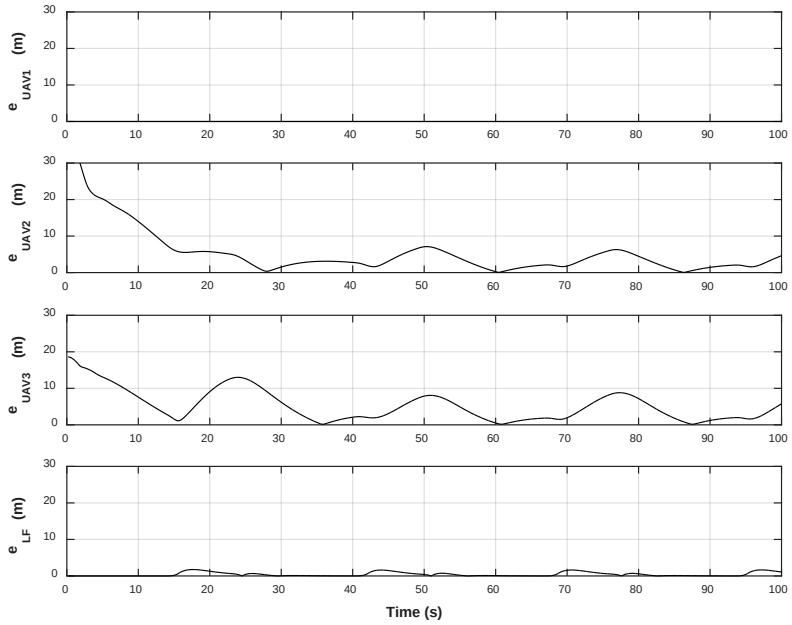

Figure 3.22: Simulation results of the suggested leader-follower formation algorithm (formation position errors @ t_{com} = 0.02 s)

The effect of the position error, which depends on the formation geometry, is also analyzed. Based on the leader's body coordination, longitudinal and lateral formation geometries are changed, and formation position errors during simulation are compared.

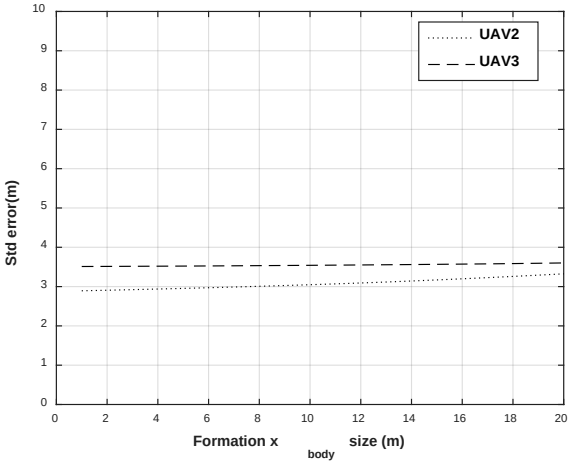

Figure 3.23: Standard deviation of position error depending on longitudinal formation distance @ $y_{body} = 15m$

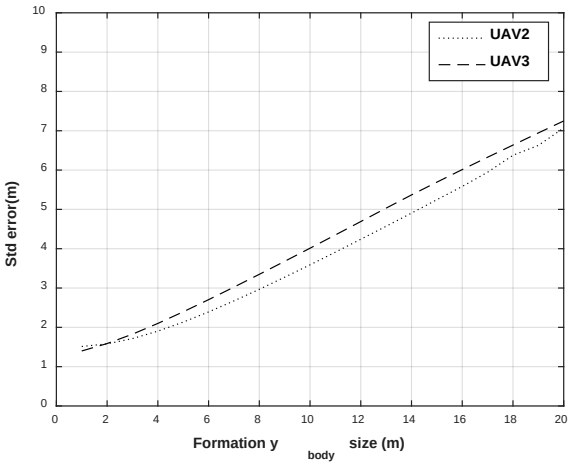

Figure 3.24: Standard deviation of position error depending on lateral formation distance @ $x_{body} = 15m$

As shown in Fig. 3.23 and Fig. 3.24, the formation position error is mainly affected by the lateral size of formation. It is because that the length of each UAV's formation path is directly proportional to the lateral size of the formation when there exists a curved path during the formation flight. Also, for the fixed-wing UAV, accelerating the UAV by increasing thrust is easier than decelerating the UAV, and therefore UAV2 (accelerating outer UAV) has the less formation error than the formation error of UAV3 (decelerating inner UAV).

To investigate the effect of communication period, t_{com} = 1 s case is simulated. Fig. 3.25 shows the trajectory result, and Fig. 3.26 shows the formation position result. Formation position errors are shown in Fig. 3.27. Although there exists large communication delay, flight paths are maintained. The communication delay generates position error along the flight path axis of the formation as shown in Fig. 3.26. Because the communication delay does not affect to formation path following, path-following performance of the leader UAV is not changed.

Table 3.5: Initial simulation parameters (the suggested Leader- follower @ t_{com} = 1.00 s)

Parameter	Value	Parameter	Value
$(p_1^n)_{initial}$	(-200,-100,60)	$(\psi_1)_{initial}$	0 deg
$(p_2^n)_{initial}$	(-240,-130,60)	$(\psi_1)_{initial}$	0 deg
$(p_3^n)_{initial}$	(-180,-130,60)	$(\psi_1)_{initial}$	0 deg
$(V_1)_{inital}$	11 m/s	t_{simul}	0.02 s
$(V_2)_{inital}$	11 m/s	t_{GNC}	0.02 s
$(V_3)_{inital}$	11 m/s	t_{com}	1.00 s

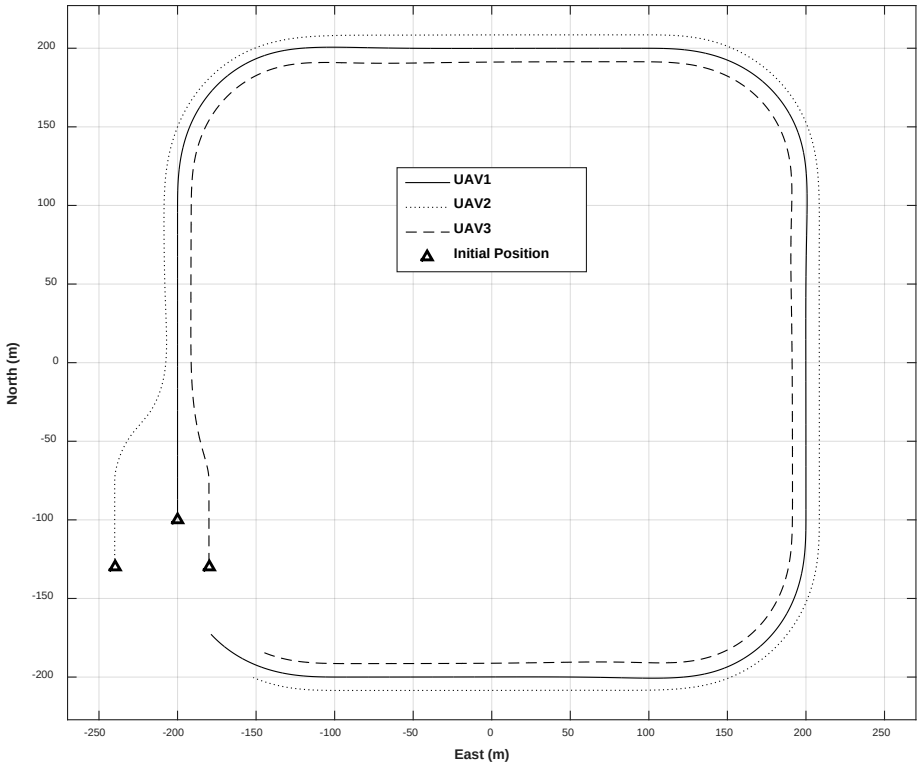

Figure 3.25: Simulation results of the suggested leader-follower formation algorithm (trajectories of UAVs @ t_{com} = 1.00 s)

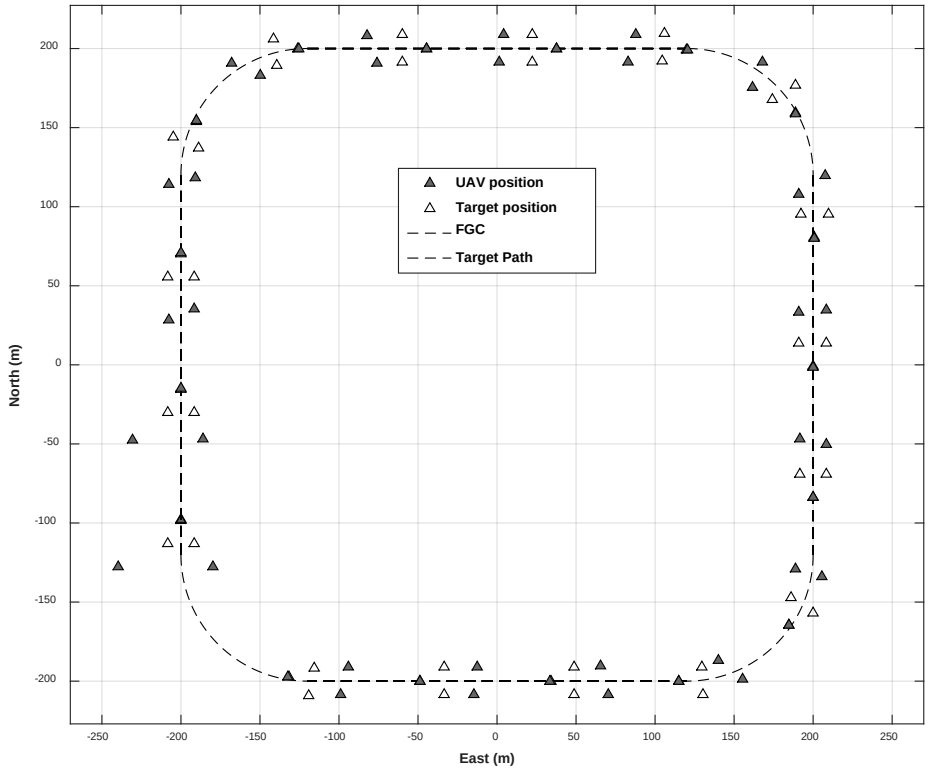

Figure 3.26: Simulation results of the suggested leader-follower formation algorithm (formation positions @ t_{com} = 1.00 s)

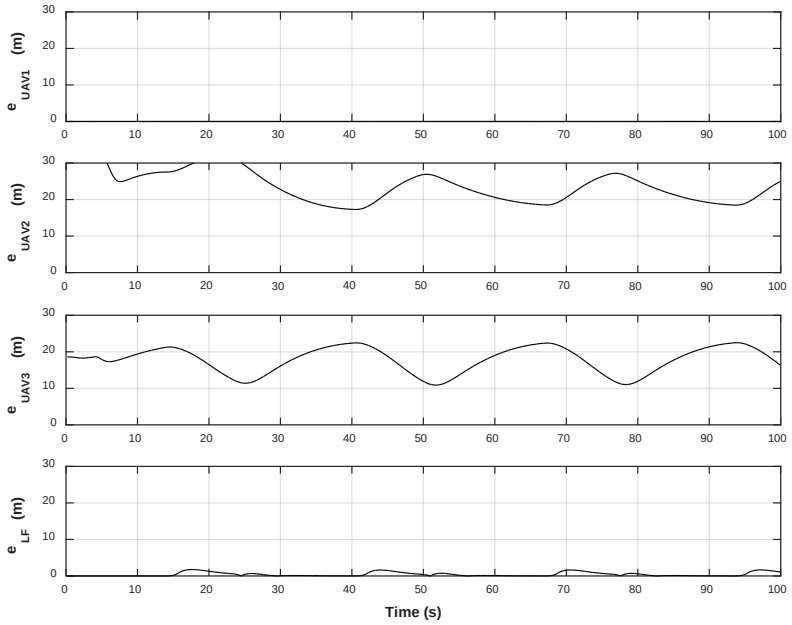

Figure 3.27: Simulation results of the suggested leader-follower formation algorithm (formation position errors @ t_{com} = 1.00 s)

Compared to the result of FGC algorithm, in case of t_{com} = 1, the proposed leader-follower algorithm provides a more stable flight path. Figure 3.28 shows the effect of communication period on the formation position error. As communication period increases, formation errors of UAVs are also increase because of inaccurate estimation of the leader's position.

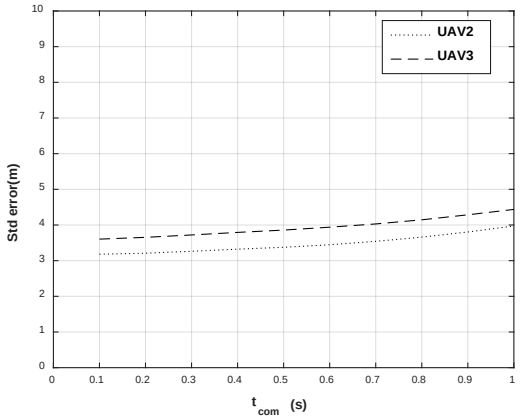

Figure 3.28: Formation position errors depending on t_{com}

To reduce the follower's position error in case of large communication delay, the leader's position should be compensated using the information of the previous flight path. UAVs are sharing their sensor information and follower UAVs know the previous leader UAV's position, the current position of the leader UAV can be estimated.

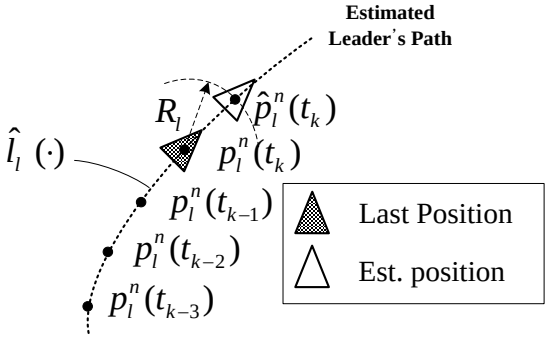

Figure 3.29: Communication delay compensation

As shown in Fig. 3.29, the current position of the leader UAV, $\hat{p}_l^n(t_k)$, is intersection point of the estimated leader's path $\hat{l}_l(\cdot)$ and R_l, i.e.,

$$\begin{aligned} &R_l = V_l \times t_{com} \\ &\text{where } \hat{p}_l^n = \begin{bmatrix} \hat{p}_{lx} & \hat{p}_{ly} \end{bmatrix}, \left\| \hat{p}_l^n - p_l^n \right\| = R_l, \text{and } \hat{p}_{ly} = \hat{l}_l(\hat{p}_{lx}). \end{aligned} \tag{3.32}$$

Once $\hat{p}_l^n(t_k)$ is obtained, follower's flight path $l_f(x)$ and guidance point $p_{L_f}^n$ can be recalculated. By this procedure, longitudinal position error can be reduced. This feature can be verified by numerical simulation. Table 3.6 summarizes the simulation parameters. By compensating the leader's position, position error of the follower UAV is effectively reduced as shown in Fig. 3.32.

Table 3.6: Initial simulation parameters (the suggested Leader- follower method @ t_{com} = 1.00 s with position estimation of UAV1)

Parameter	Value	Parameter	Value
$(p_1^n)_{initial}$	(-200,-100,60)	$(\psi_1)_{initial}$	0 deg
$(p_2^n)_{initial}$	(-240,-130,60)	$(\psi_1)_{initial}$	0 deg
$(p_3^n)_{initial}$	(-180,-130,60)	$(\psi_1)_{initial}$	0 deg
$(V_1)_{inital}$	11 m/s	t_{simul}	0.02 s
$(V_2)_{inital}$	11 m/s	t_{GNC}	0.02 s
$(V_3)_{inital}$	11 m/s	t_{com}	1.00 s

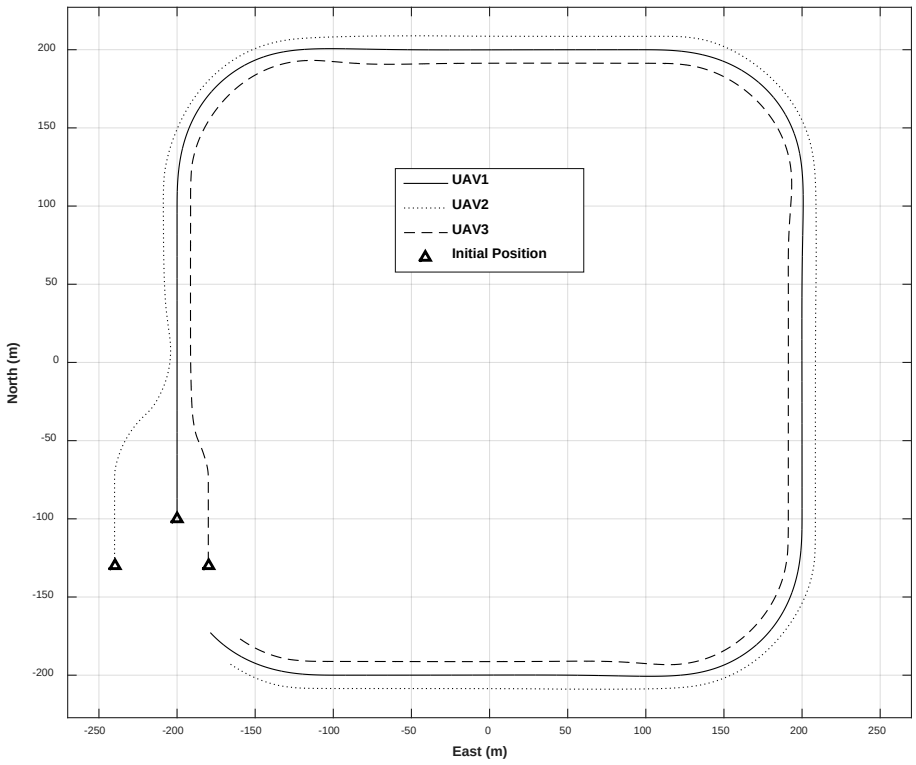

Figure 3.30: Simulation results of the suggested leader-follower formation algorithm (trajectories of UAVs @ t_{com} = 1.00 s with position estimation of UAV1)

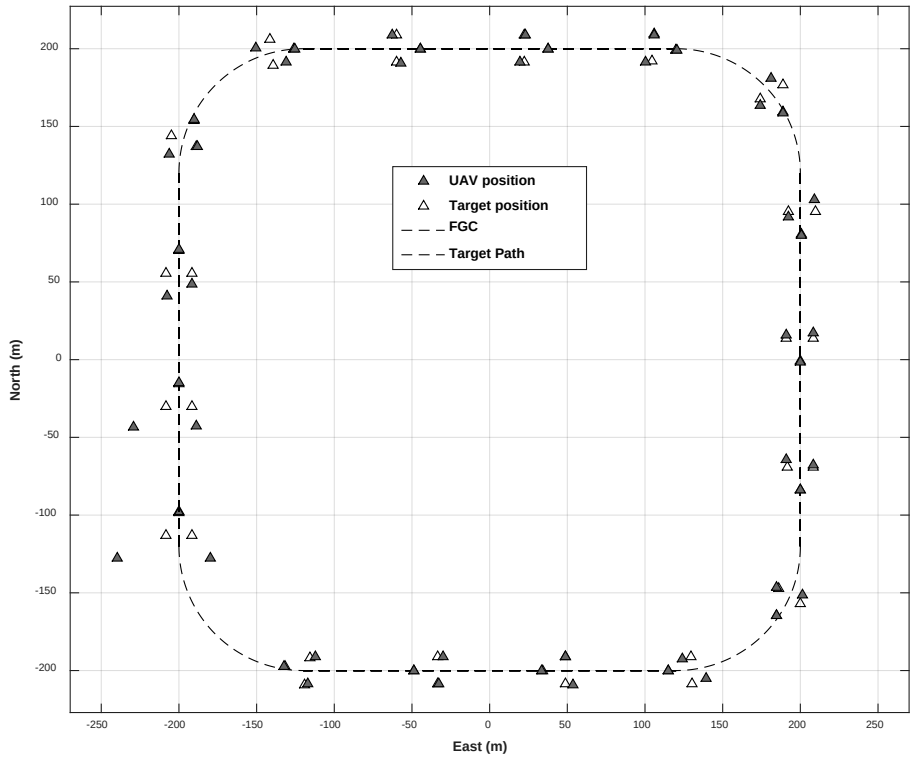

Figure 3.31: Simulation results of the suggested leader-follower formation algorithm (formation positions @ t_{com} = 1.00 s with position estimation of UAV1)

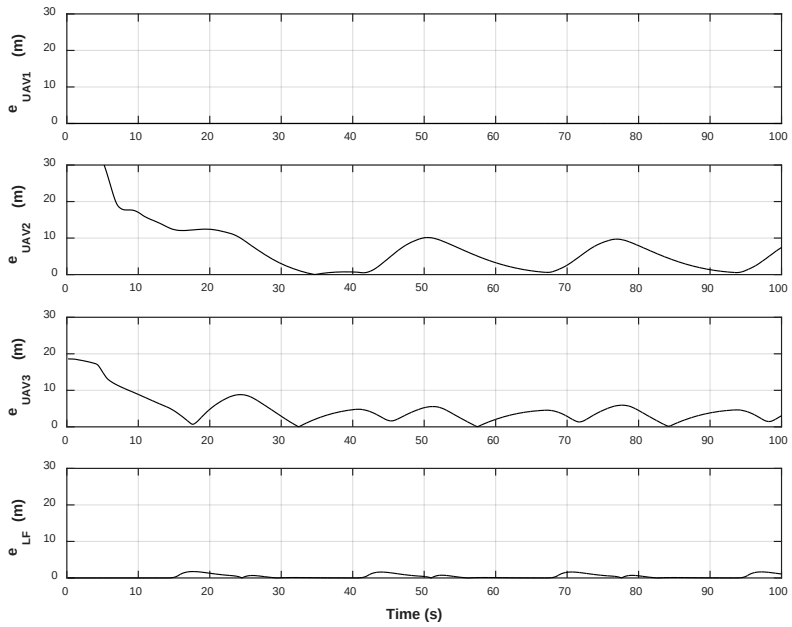

Figure 3.32: Simulation results of the suggested leader-follower formation algorithm (formation position errors @ t_{com} = 1.00 s with position estimation of UAV1)

For the case that the estimation of the leader's position is applied, the result of the formation position error is shown in Fig. 3.33. It shows that the error is maintained within the error of the initial position.

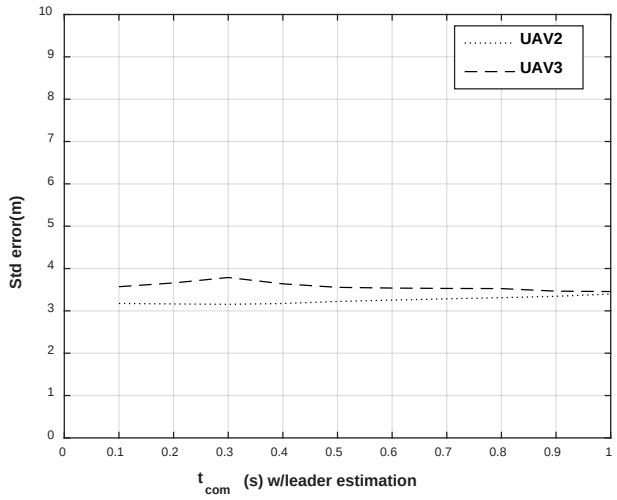

Figure 3.33: Formation position errors depending on communication period with position estimation of the leader UAV

In summary, compared to the proposed FGC algorithm, the proposed leader-follower formation algorithm is more suitable for the close formation flight even in the case that the communication delay exists. Based on the numerical simulation result, the proposed leader-follower formation flight guidance can be verified by the integrated formation flight test.

4. Integrated Formation Flight Simulation

Developed formation flight algorithms have been validated by integrated formation flight simulation. For effectively demonstrating the algorithm, the integrated formation flight scenarios is designed which is consisted of multiple formation.

4.1 Procedure for Autonomous Formation Flight

The integrated formation flight that consists of area monitoring and formation movement is conducted to demonstrate the performance of the formation flight guidance laws. In the monitoring mission, the UAVs circle the area based on the circular formation flight guidance. And for the formation flight mission, the UAVs fly closely in a triangular formation as they move to the next target point area.

The integrated formation flight is composed of five subscenarios, which are conducted in sequence. Table 4.1 summarizes the formation flight scenarios considered in this study. Each scenario has a specified Mission and Stage number depending on the longitudinal and lateral guidance mode. The mission variable specifies the observation or movement scenario, and the stage variable addresses the guidance mode transition. During the integrated formation flight, the stage variable is automatically changed based on the consensus of the UAVs. Figure 4.1 shows the path description of the integrated formation flight scenarios. Five subscenarios are described below.

Table 4.1: The integrated formation flight scenarios

Scenario	Maneuver	Mission	Stage	Longitudinal guidance	Lateral guidance
-	Sequential takeoff	-	-	-	-
1	Circular formation/ Separated altitude	1	1,2	$360 / N_1$ deg phase separation/ $\delta h = \pm 10$ m	Circular path following approximately 1st target
2	Circular formation/ Same altitude	1	3	$360 / N_1$ deg phase separation/ $\delta h = 0$ m	Circular path following approximately 1st target
3	Separation and Reconfiguration of Circular formation	1	4,5	$360 / N_2$ deg phase separation/ $\delta h = 0$ m	Transition from 1st target to 2nd target
4	Close circular formation	1	6	30 deg phase separation/ $\delta h = 0$ m	Circular path following approximately 2nd target
5	Close triangular formation	2	-	-15 m rear position of leader UAV/ $\delta h = 0$ m .	$\mp 5\sqrt{3}$ m left/right position of leader UAV
-	Sequential landing	-	-	-	-

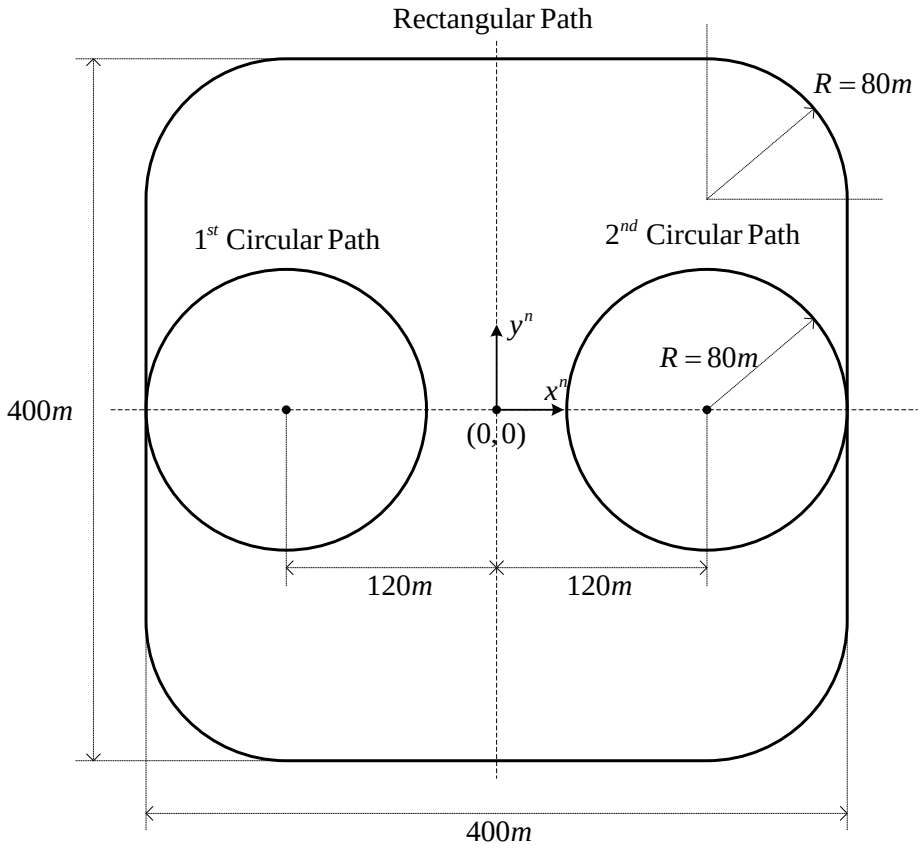

Figure 4.1: A flight path description of the integrated formation flight scenarios

4.1.1 Circular Formation Flight with Separated Altitude

In the flight experiment, takeoff and landing are manually conducted by human pilots. Three UAVs takeoff in sequence, and the manual mode of each UAV is immediately switched to autonomous formation flight mode when it reaches the reference height. To prevent collisions between the UAVs during takeoff, each UAV follows a circular path with an altitude difference δh. The reference altitude is $\mathrm{UAV1} = 60\,m$, and the altitude difference between UAV2 and UAV3 is set as $\delta h = \pm 10\,m$; therefore, the target altitude of UAV2 is $50\,m$, and that of UAV3 is $70\,m$ (Stage 1). During the separated altitude flight, the relative phase angles among UAVs are regulated to $360 / N_1 \deg$, where N_1 is a number of UAVs. The relative phase angles are controlled by the circular formation flight guidance law. If all three UAVs are on the circular path with $120 \pm 10 \deg$ phase angles (Stage 2), then UAV2 and UAV3 move to the reference altitude $60\,m$ by increasing/decreasing their altitude by using a flight path angle control.

4.1.2 Circular Formation Flight at the Same Altitude

During the altitude transitions, the phase angles among the UAVs may change because of the acceleration of UAV3 and the deceleration of UAV2. Phase angle formation flight guidance regulates the phase angles of the UAVs to be $120 \pm 10 \deg$ (Stage 3). In this scenario, omni-directional surveillance of the target can be performed, wherein the target is at the center of the circular path.

4.1.3 Separation and Reconfiguration Formation Flight

To monitor multiple areas, the UAVs on the circular path should be separated and move to the second target. In the separation stage (Stage 4), the UAVs fly

from the 1st circular path to the 2nd circular path one by one. During the separation, the phase angles of the remaining UAVs are modified to the phase angle of $360/N_1 \deg$, where N_1 is the number of UAVs remaining. In the reconfiguration stage (Stage 5). UAVs on the 2nd circular path are reconfigured to maintain a phase angle of $360/N_2 \deg$, where N_2 is the number of the UAVs in the 2nd circular path. In this stage, UAVs can monitor multiple areas while the circular formation flight is performed.

4.1.4 Close Circular Formation Flight

After the UAVs complete monitoring of the mission area, they should fly together to the next mission area while maintaining the close formation. To perform this task, the UAVs on the circular path should converge to a close formation. To accomplish this maneuver, the phase angles between the UAVs are adjusted to 30 ± 10 deg (Stage 6). Once the specified phase angle has been reached, the circular formation flight mode is switched to the close formation flight mode.

4.1.5 Close Triangular Formation Flight

The close formation flight guidance law makes three UAVs follow a prescribed path, while keeping them in a triangular formation. In the triangular configuration, UAV1, UAV2, and UAV3 are located at $(0m, 0m)$, $(-15m, 5\sqrt{3}m)$, and $(-15m, -5\sqrt{3}m)$, respectively. UAV1 becomes the reference leader UAV, which tracks the predefined path, and the other UAVs become follower UAVs. The formation path of the followers can be calculated based on the leader's path. To ensure collision avoidance, a safety radius of $10m$ is considered for each of the following UAVs. If one of the follower UAV's relative distance becomes less than $10m$, then an additional lateral

command is activated to make the follower UAV fly at a distance from the formation.

4.2 Simulation Results

The proposed integrated formation flight scenario is composed of switching logics and multiple formation flights. The algorithms are thoroughly examined using a 6-DOF numerical simulation in the MATLAB/Simulink environment. The identical integrated formation flight guidance block is used in all UAVs' embedded software with the assigned UAV number. The numerical simulation results are shown in Fig. 4.2, which indicates that the formation flight of multiple UAVs is performed well using both the close formation flight algorithm and close formation flight algorithm.

Table 4.2: Initial parameters of the integrated formation flight simulation

Parameter	Value	Parameter	Value
$(p_1^n)_{initial}$	(-250,0,60)	$(\psi_1)_{initial}$	0 deg
$(p_2^n)_{initial}$	(-250,100,50)	$(\psi_2)_{initial}$	0 deg
$(p_3^n)_{initial}$	(-250,-100,70)	$(\psi_3)_{initial}$	0 deg
$(V_1)_{inital}$	11 m/s	t_{simul}	0.02 s
$(V_2)_{inital}$	11 m/s	t_{GNC}	0.02 s
$(V_3)_{inital}$	11 m/s	t_{com}	0.10 s

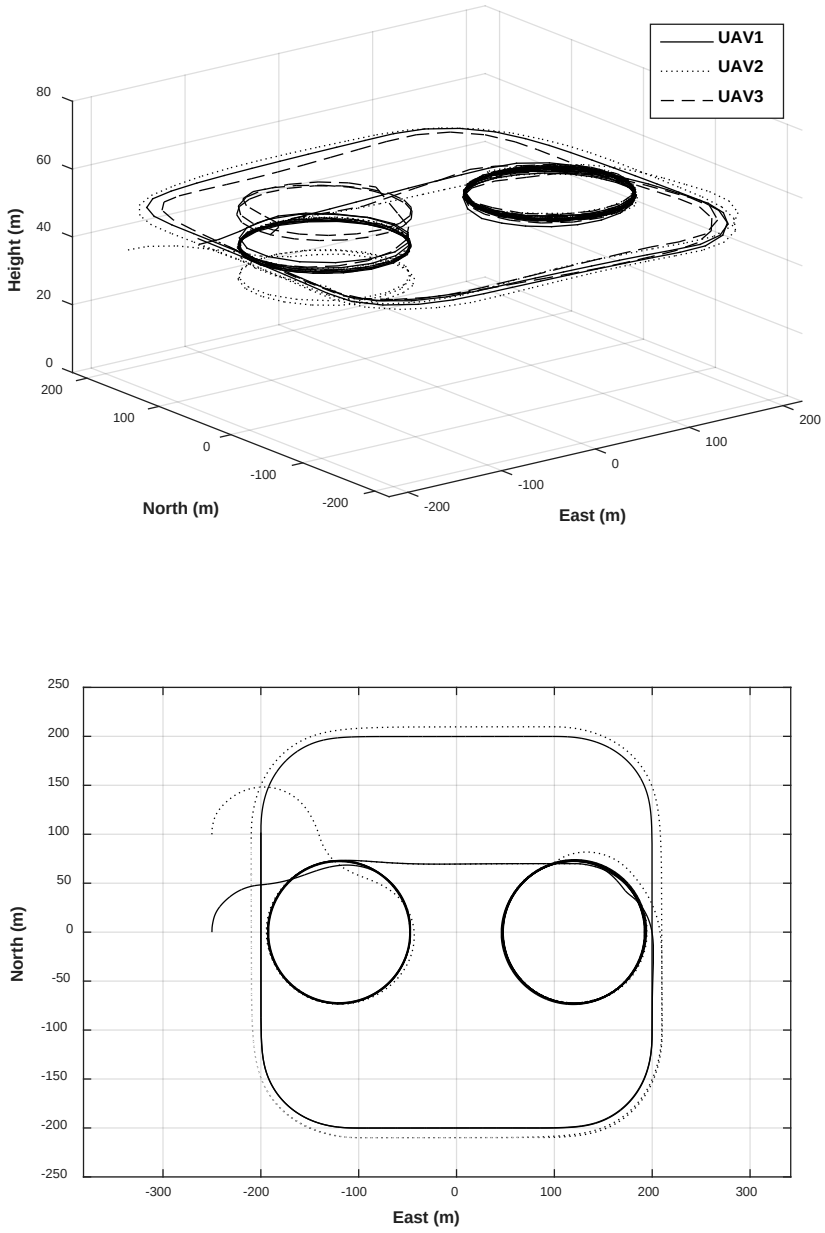

Figure 4.2: 2D and 3D simulation results of the integrated formation flight

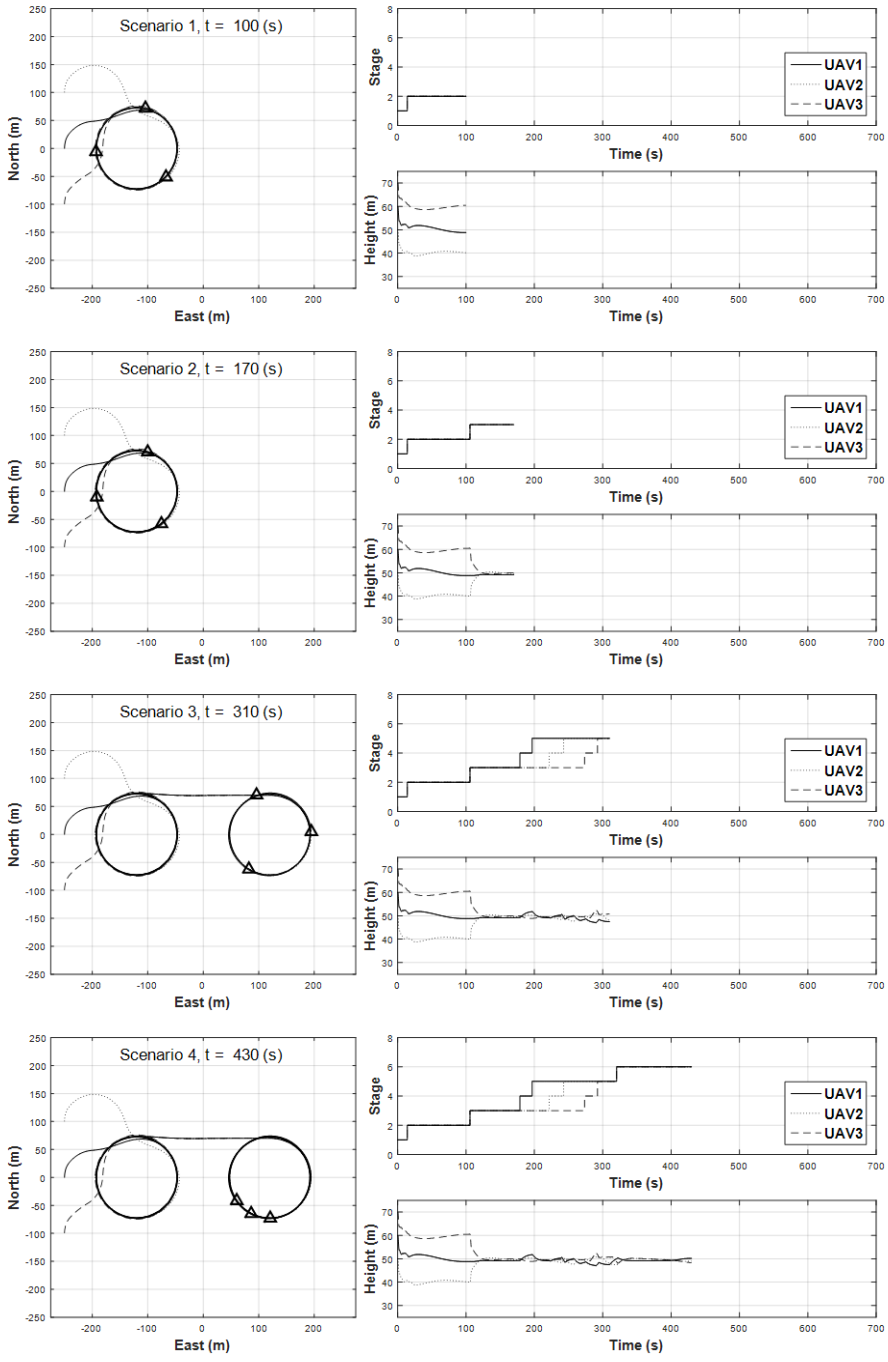

Figure 4.3: Simulation results of the circular formation flight

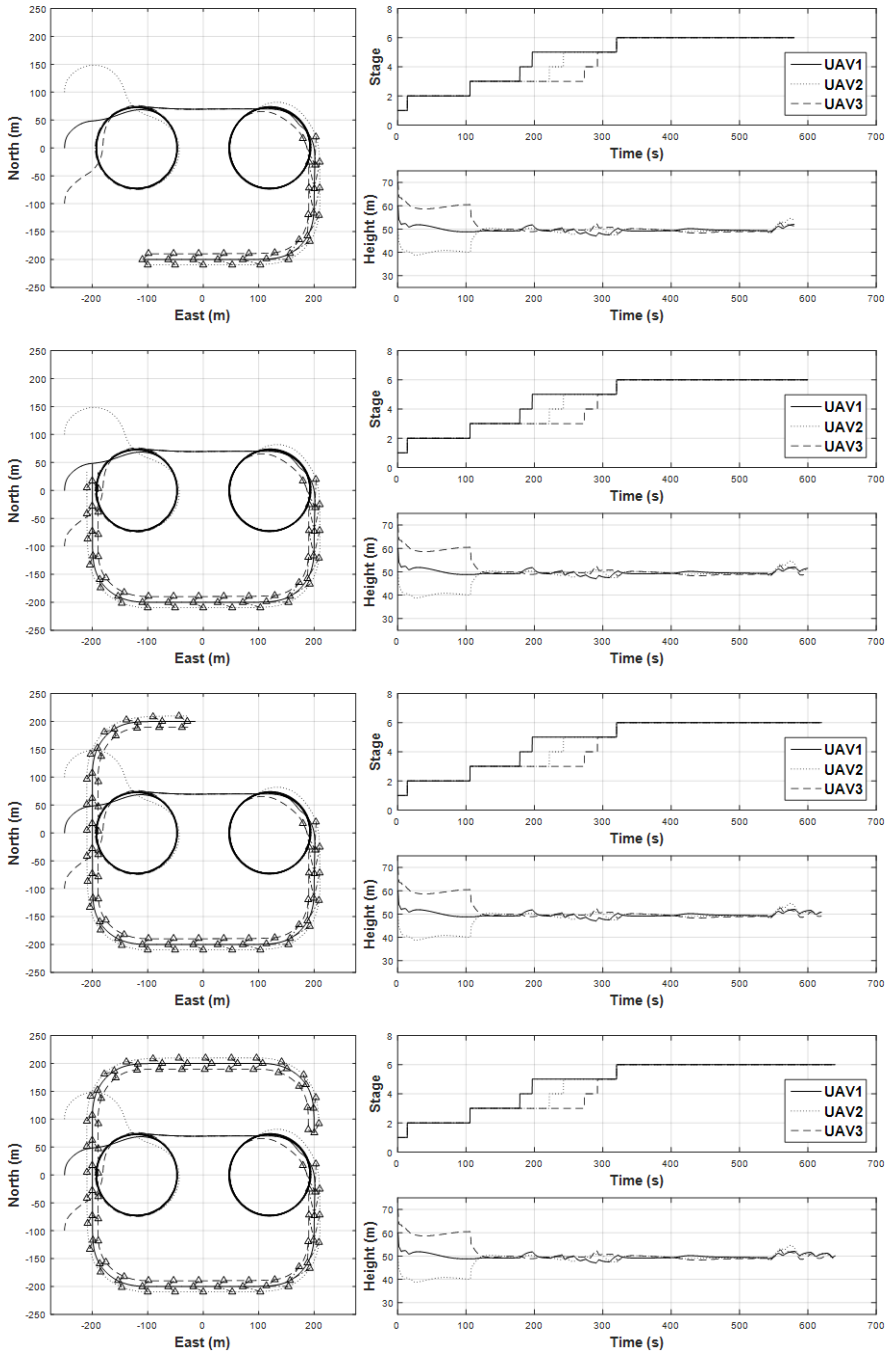

Figure 4.4: Simulation results of the close triangular formation flight

5. Experimental Result

After demonstrating the performance of the proposed algorithm via numerical simulation, a flight test is performed using the developed multiple UAV system[1].

The integrated formation flight scenario as summarized in Table 4.1 is conducted in sequence. The Mission and State variables are sequentially and automatically changed. The fight test is conducted in an area that measures $400\,m \times 400\,m$, and the results are shown below. In Fig. 5.1-Fig. 5.3, solid, dotted, and dashed lines correspond to the trajectories of UAV1, UAV2, and UAV3, respectively. During the sequential takeoff stage as shown in Fig. 5.1(a), the UAVs form a 120-degree circular formation at different altitudes to ensure safety as shown in Fig. 5.1(b). Once the phase angle of the circular formation is stabilized, UAV2 and UAV3 move to the same altitude, $60\,m$, and execute circular formation flight as shown in Fig. 5.1(c). After performing a circular formation flight along the circular path, UAV1 is separated from the formation and moves to the next circular path, and UAV2 and UAV3 continue the circular formation of 180 degrees along the 1st circular path and UAV2 moves to the 2nd circular path and reconfigures the 180-degree circular formation with UAV1 as shown in Fig. 5.2(a) at the 2nd circular path. Next, UAV3 moves to the 2nd circular path, and finally, the UAVs reconfigure the circular formation of 120 degrees as shown in Fig. 5.2(b). The UAVs reduce the phase angles to 30 degrees to prepare for close formation flight as shown in (Fig. 5.2(c); then, they start the close formation flight as shown in Fig. 5.3(a), and the UAVs perform the close triangular formation flight as shown in Fig. 5.3(b). After formation flight scenarios ending, sequential landing as shown in Fig. 5.3(c) is conducted.

[1] Video of the flight test is available at https://goo.gl/0ekRE3

A detailed triangular formation flight result is shown in Fig. 5.4. As shown in Fig. 5.4, UAV1 follows the rounded rectangular path, and the follower UAVs generate their own formation path based on the estimated path of UAV1. Due to the east wind effect, the formation paths of UAV2 and UAV3 are slightly shifted to the west; nevertheless, the triangular shape is maintained well during the formation flight. The position histories of the integrated formation flight are shown in Fig. 5.5. The mode variable indicates a flight mode controlled by an RC controller, where Mode 0 is the manual flight mode, Mode 1 is the stabilized co-pilot flight mode, and Mode 2 is the autonomous formation mission flight mode. Depending on the status of the UAVs, the stage of each UAV may be different. The circular formation flight starts at 230s, and the triangular formation flight starts at 591s. The lateral and longitudinal control histories are shown in Fig. 5.6. As shown in Fig. 5.6, the inner-loop controllers perform well to follow the guidance commands.

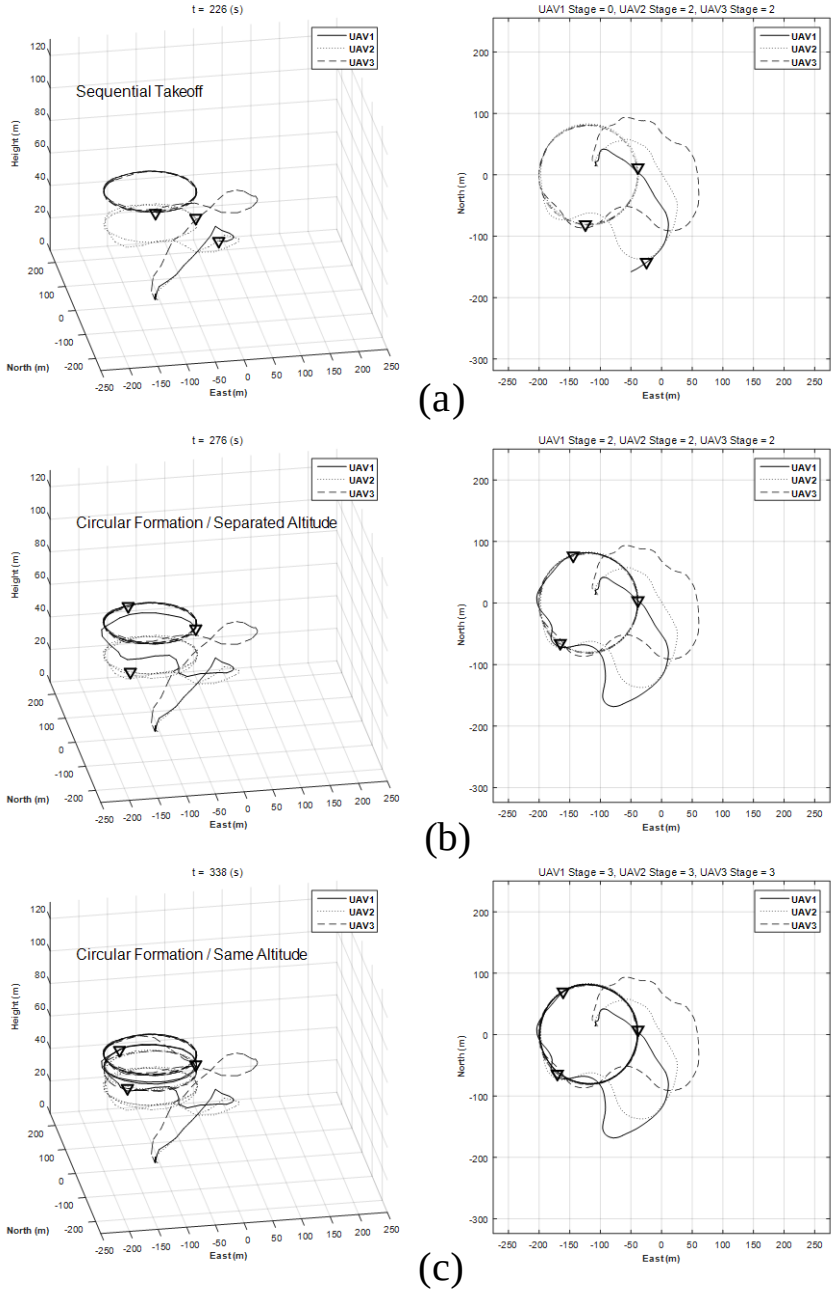

Figure 5.1: 2D and 3D results of the integrated formation flight test (a) Sequential takeoff, (b) Circular formation with separate altitude, (c) Circular formation with same altitude

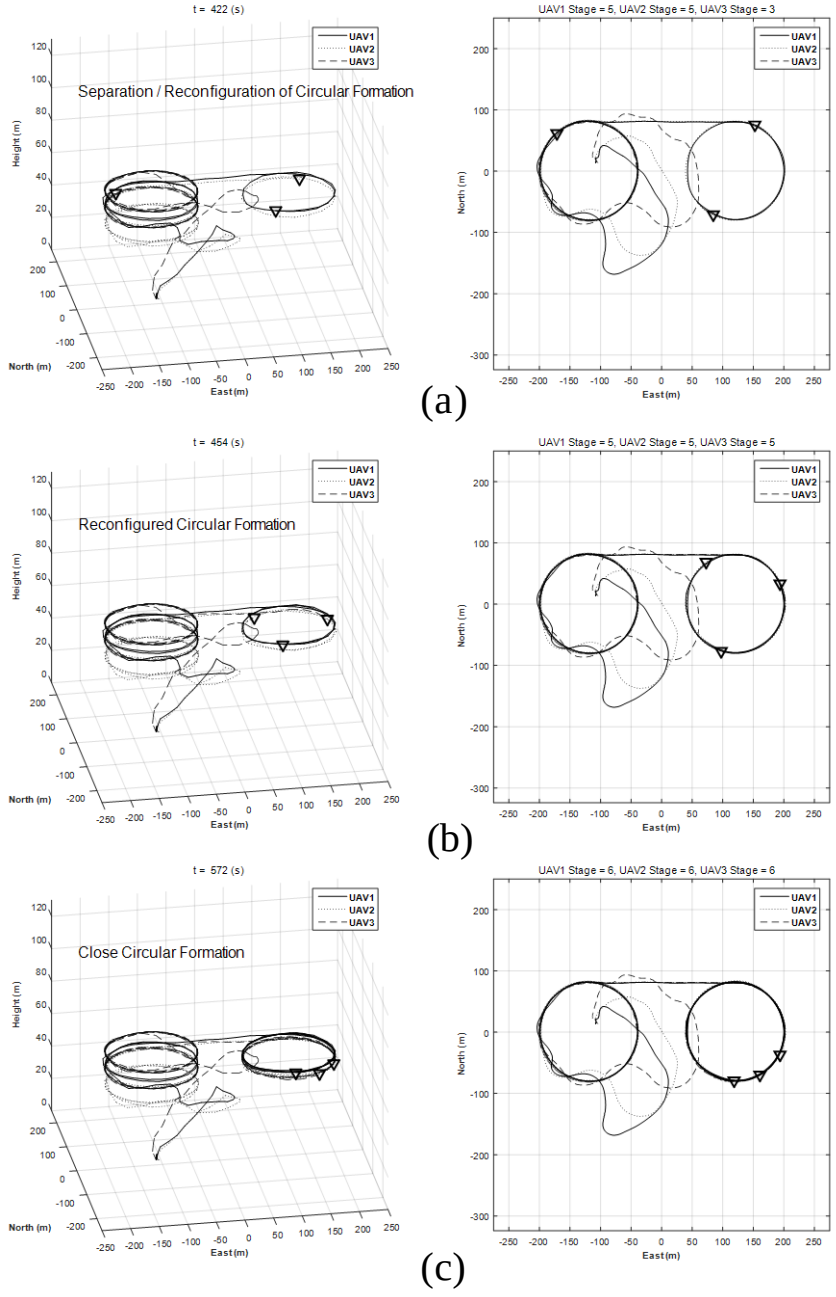

Figure 5.2: 2D and 3D results of the integrated formation flight test (a) Separation and reconfiguration of circular formation, (b) Reconfiguration of circular formation, (c) close circular formation

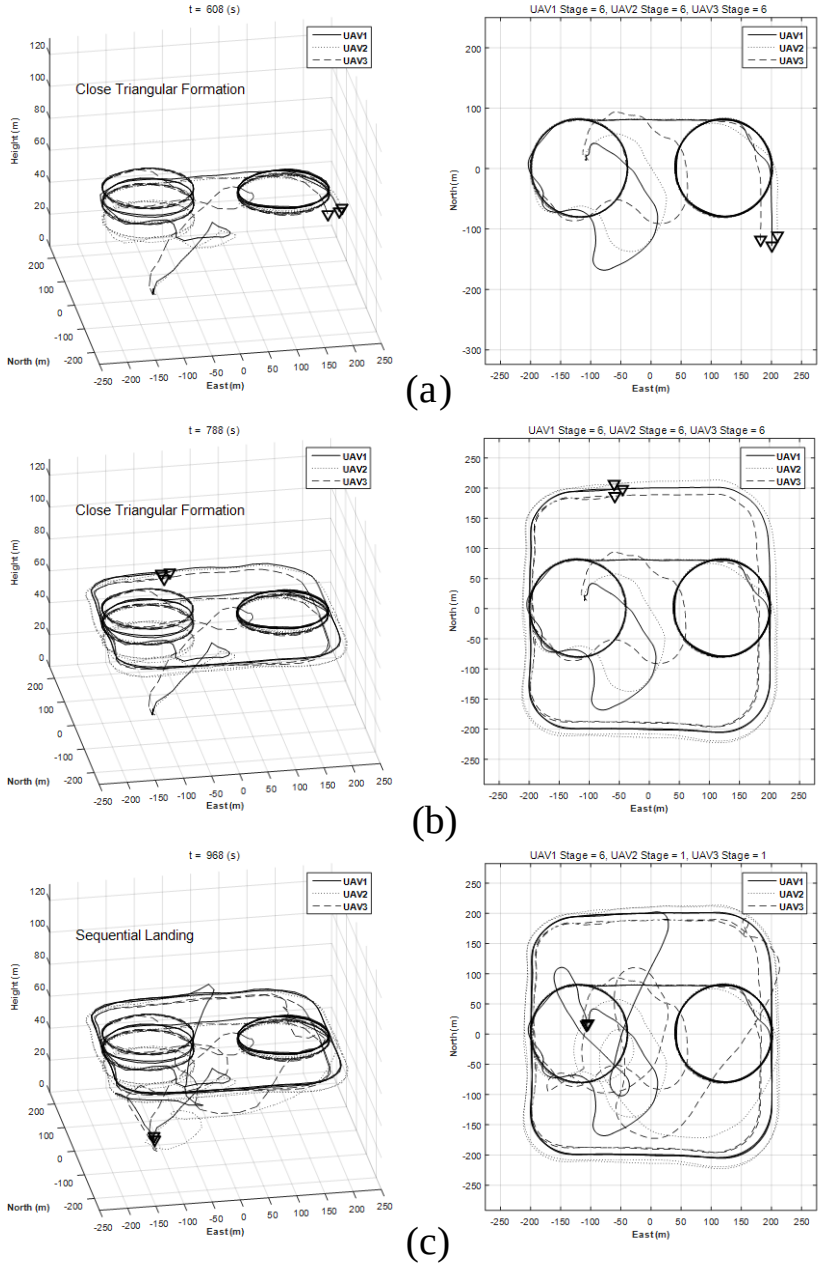

Figure 5.3: 2D and 3D results of the integrated formation flight test (a) Transition to close formation, (b) Close triangular formation, (c) Sequential landing

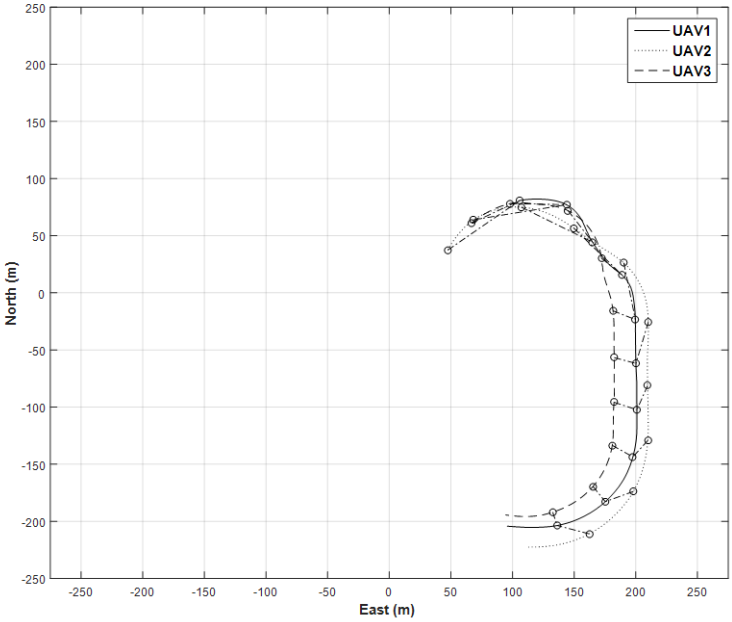

(a) t = 620 sec

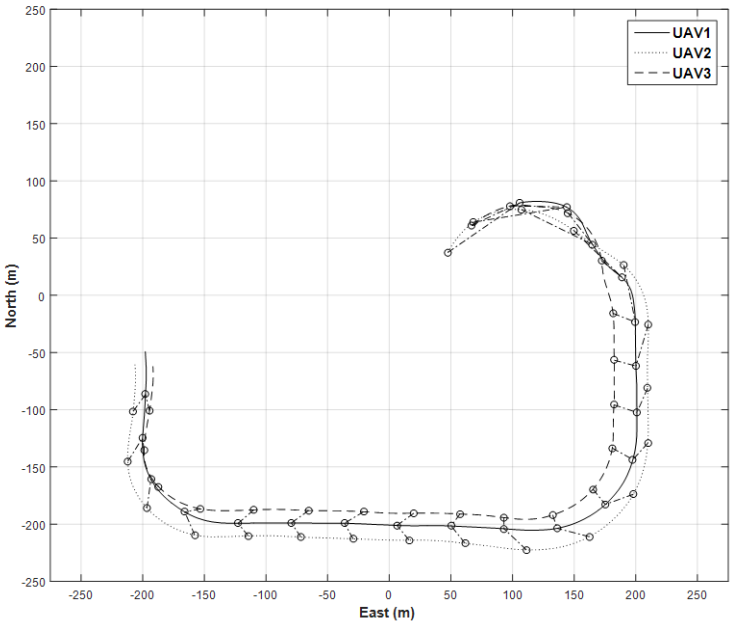

(b) t = 650 sec

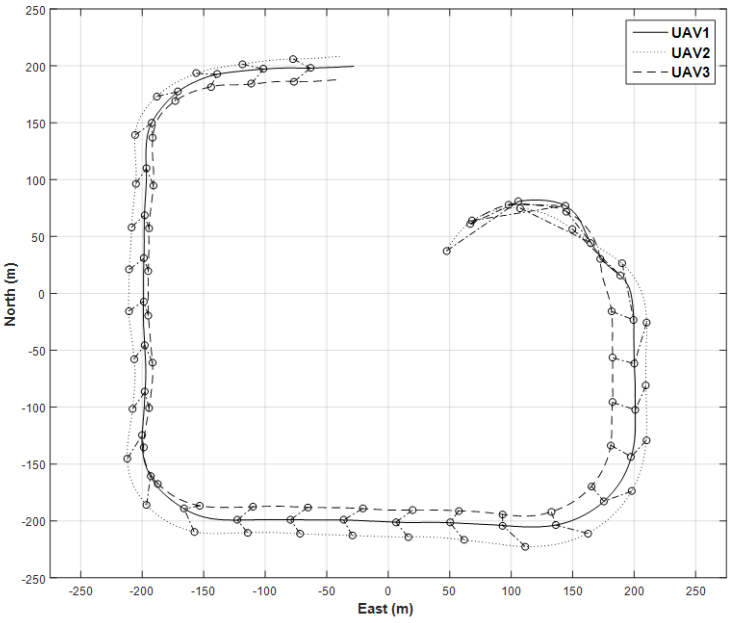

(c) t = 680 sec

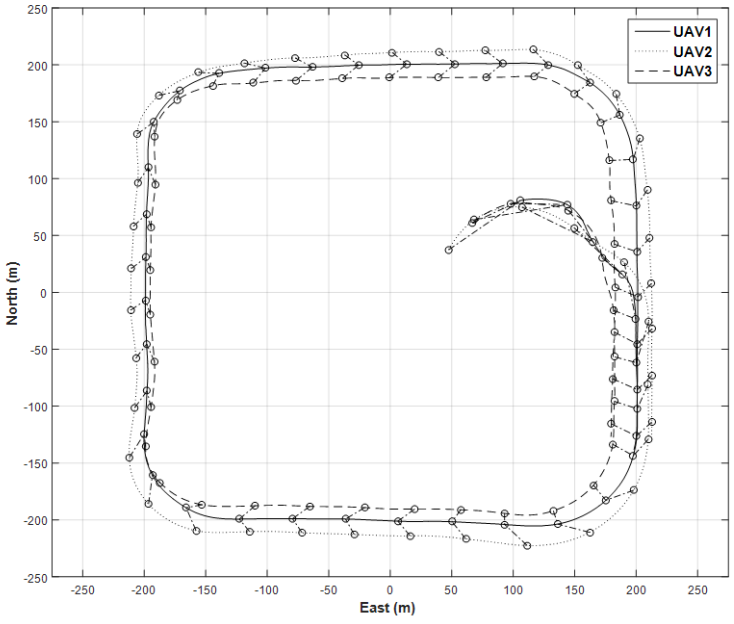

(d) t = 720 sec

Figure 5.4: Detail results of the close triangular formation flight

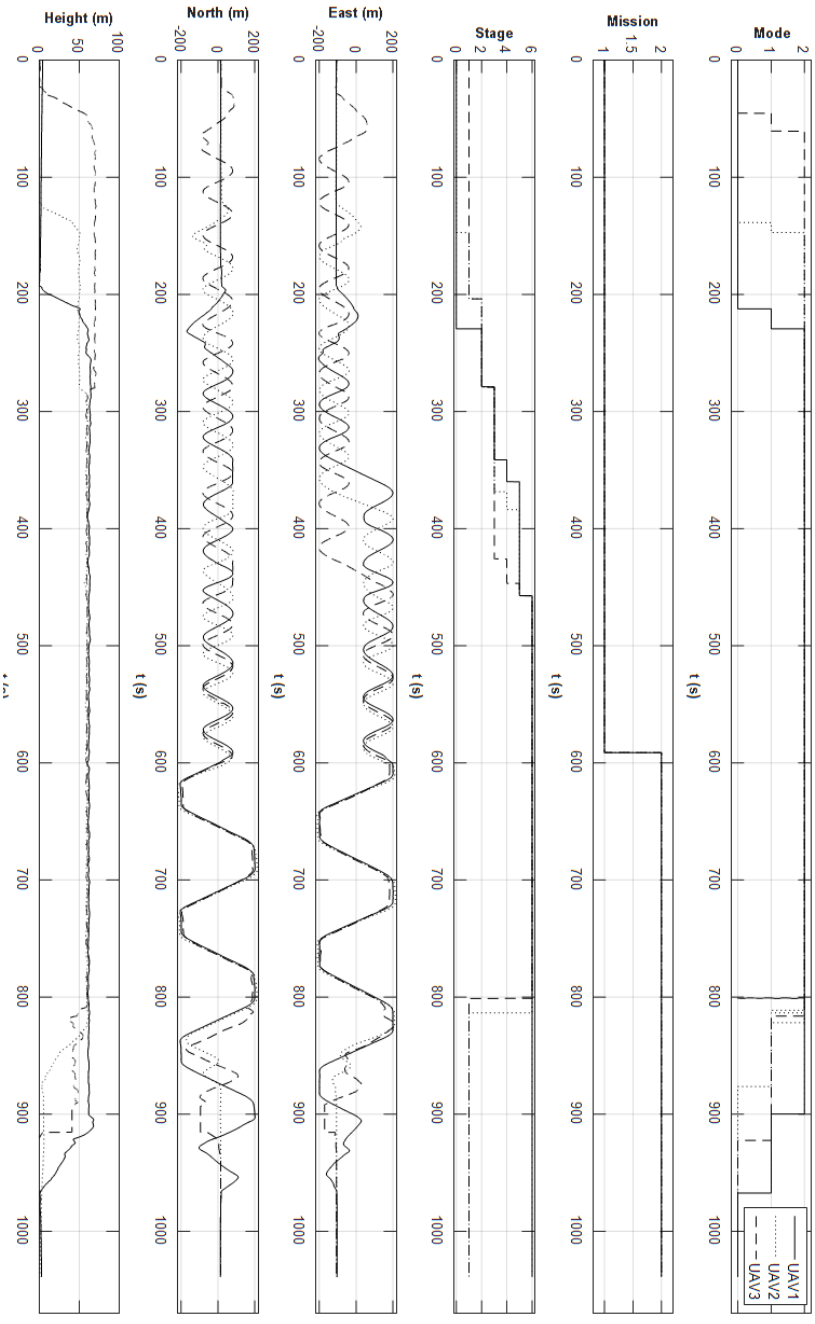

Figure 5.5: Position histories of the integrated formation flight

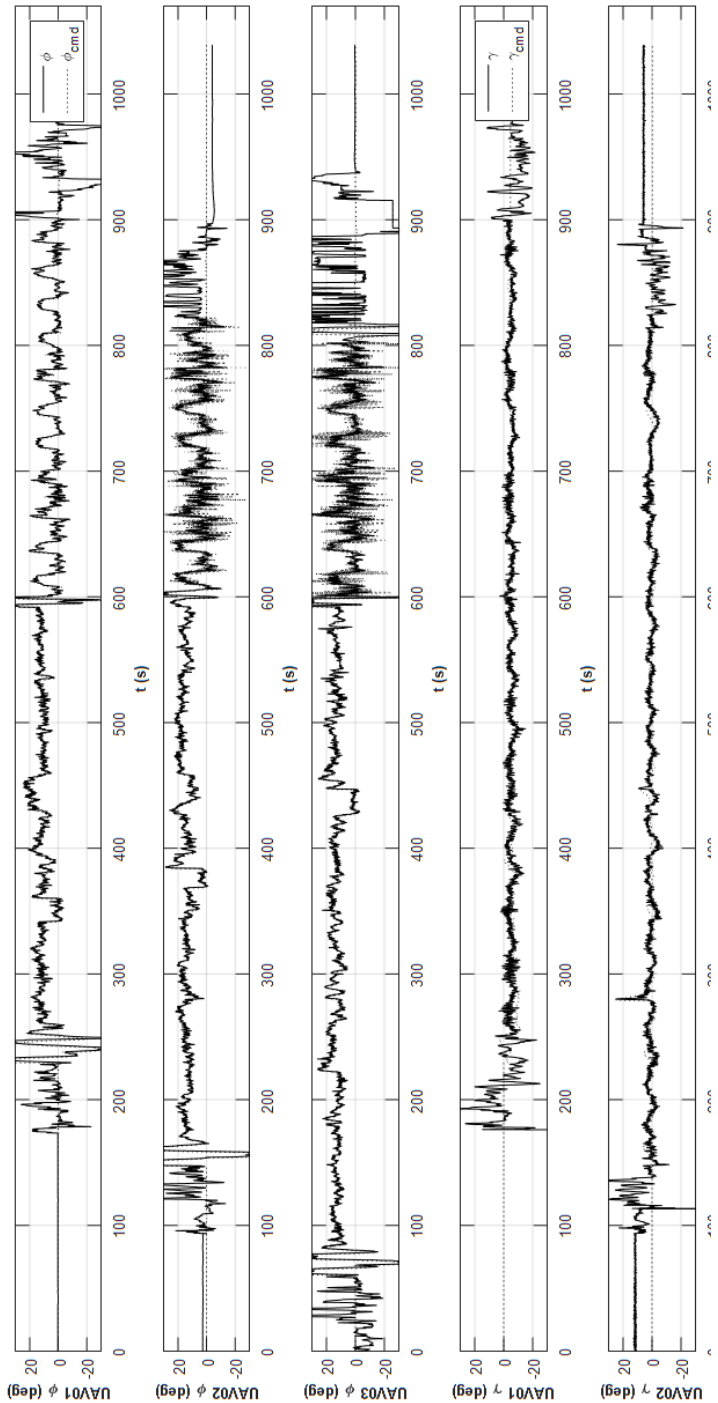

Figure 5.6: Command histories of the integrated formation flight

Figure 5.7shows the site of the flight test with the UAVs, and Fig. 5.8 shows the photo of the close formation flight using three UAVs in a triangular formation captured by a ground camera. The triangular formation is shown to be maintained well during the flight test.

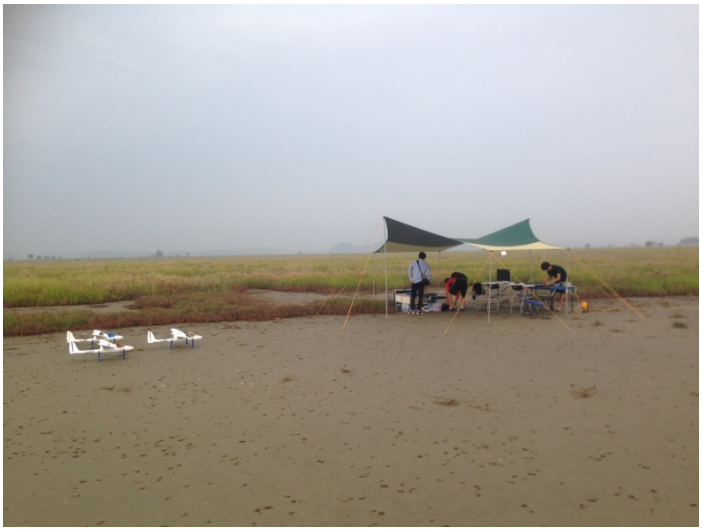

Figure 5.7: Flight experiment setup

Figure 5.8: Multiple UAVs in close triangular formation

6. Conclusion

6.1 Concluding Remarks

In this dissertation, formation flight guidance algorithms for the formation flight of three fixed-wing UAVs were proposed, and the performance of the proposed algorithms was verified using numerical simulations and an actual flight test. The formation flight performed by three fixed-wing UAVs was based on circular formation flight guidance and close formation flight algorithm.

A multiple UAV system was developed with identical performance under consideration. The avionics system developed was based on a customized embedded FGC to enable decentralized communication in the limited space available in a small UAV. The decentralized onboard sensor information-sharing system for miniature UAV systems was developed using ZigBee modems. With the ZigBee modems, which support a multipoint-to-multipoint communication topology, sequential cyclic communication without a centralized ground control system was realized by accurately managing the communication timing. The performance of the decentralized communication system was verified by an analysis of the communication delays among the UAVs. The resulting UAV dynamics were identified using a system identification scheme, which was implemented in the simulated multiple UAV environment.

Guidance laws for circular formation flight and close formation flight were proposed. The phase angle control scheme was used for circular formation flight and for formation separation and reconfiguration scenarios. The close formation flight algorithm was based on the geometric center and leader-follower methods. Both approaches were developed for formation flight, and the effect of the communication delay was analyzed. A leader-follower guidance law was used for the close triangular formation flight that occurred during a formation movement based on the results of the numerical simulation.

The proposed guidance laws were examined using a 6 DOF numerical simulation, and an actual flight test was conducted using the developed multiple UAV system. To verify the proposed algorithms for a complete formation flight, an integrated formation flight scenario was designed, and various formation flights were performed in sequence. A circular formation flight, including sequential takeoffs, was performed, and then, a close triangular formation flight was performed. The results of the flight test showed that the autonomous integrated formation flight was successfully performed.

6.2 Future Research Directions

Based on the proposed formation flight algorithms and the results of the integrated formation flight, the following topics are suggested for future studies:

- Applying formation flight guidance to rotary-wing UAVs: The suggested formation flight algorithm is based on path-following guidance, but it can also be applied to rotary-wing UAV formation flight. A rotary-wing UAV has more longitudinal maneuverability than a fixed-wing UAV. Therefore, in close formation flight, rotary-wing UAVs can easily follow the speed commands that are generated according to their geometrical positions in the formation. Consequently, their ability to maintain the formation will improve.

- Three-dimensional formation flight guidance: A formation path can be extended to three-dimensional space. In this case, the path estimation and follower path generation algorithms should consider the height of the path, and the guidance algorithm should be extended to handle three-dimensional movement. Because there are major differences between the longitudinal and lateral axes, the guidance algorithm should cover this dynamic difference to enable precise formation flight.

Bibliography

[1] F. Giulietti, L. Pollini, and M. Innocenti, "Formation Flight Control: A Behavioral Approach," *AIAA Guidance, Navigation, and Control Conference*, Montreal, QC, Canada, May 2007.

[2] C. Price, "The Virtual UAV Leader," in *AIAA Infotech*, Rohnert Park, CA, May 2007.

[3] N. Li and H. Liu, "Multiple UAVs Formation Flight Experiments Using Virtual Structure and Motion Synchronization," *AIAA Guidance, Navigation, and Control Conference*, Chicago, IL, August 2009.

[4] R. Teo, J. Jang, and C. Tomlin, "Automated Multiple UAV Flight—The Stanford Dragon Fly UAV Program," *43rd IEEE Conference on Decision and Control*, Atlantis, Paradise Island, Bahamas, December 2004.

[5] A. Verma, C. Wu, and V. Castelli, "UAV Formation Command and Control Management," *2nd AIAA Unmanned Unlimited System, Technologies, and Operations*, San Diego, CA, September 2003.

[6] L. Schmitt and W. Fichter, "Collision-Avoidance Framework for Small Fixed-Wing Unmanned Aerial Vehicles," *Journal of Guidance, Control, and Dynamics*, Vol. 37, No. 4, 2014, pp. 1323–1328.

[7] R. Beard, T. McLain, D. Nelson, D. Kingston, and D. Johanson, "Decentralized Cooperative Aerial Surveillance Using Fixed-Wing Miniature UAVs," *IEEE Proceedings*, Vol. 94, No. 7, 2006, pp. 1306–1324.

[8] Z. Mahboubi, Z. Kolter, T. Wang, and G. Bower, "Camera Based Localization for Autonomous UAV Formation Flight," *AIAA Infotech*, St. Louis, MO, March 2011.

[9] H. Lee, S. Moon, W. Kim, and H. Kim, "Cooperative Surveillance and Boundary Tracking with Multiple Quadrotor UAVs," *Journal of Institute of Control, Robotics and Systems,* Vol. 19, No. 5, 2013, pp. 423–428.

[10] B. Geoffrey, M. Ted, L. Michael, M. Mark, and B. Joseph, "“Mini UAVs” for Atmospheric Measurements," *AIAA Infotech*, Rohnert Park, CA, May 2007.

[11] S. Kim, H. Oh, and A. Tsourdos, "Nonlinear Model Predictive Coordinated Standoff Tracking of Moving Ground Vehicle," *AIAA Guidance, Navigation, and Control Conference*, Portland, OR, August 2011.

[12] T. Yamasaki, S. Balakrishnan, and H. Takano, "Coordinated Standoff Flights for Multiple UAVs via Second-Order Sliding Modes," *AIAA Guidance,Navigation, and Control Conference, Kissimmee*, FL, January 2015.

[13] S. Venkataramanan and A. Dogan, "A Multi-UAV Simulation for Formation Reconfiguration," *AIAA Modeling and Simulation Technologies Conference, Providence*, RI, August 2004.

[14] S. Bayraktar, G. Fainekos, and G. Pappas, "Experimental Cooperative Control of Fixed-Wing Unmanned Aerial Vehicles," *IEEE Conference on Decision and Control*, Los Angeles, CA, December 2004.

[15] Y. Gu, B. Seanor, G. Campa, M. Napolitano, L. Rowe, S. Gururajan, and S. Wan, "Design and Flight Testing Evaluation of Formation Control Laws," *IEEE Transactions on Control Systems Technology,* Vol. 14, No. 6, 2006, pp. 1105–1112.

[16] I. Maza, K. Kondak, M. Bernard, and A. Ollero, "Multi-UAV Cooperation and Control for Load Transportation and Deployment," *Journal of Intelligent & Robotic Systems,* Vol. 57, 2010, pp. 417–449.

[17] N. Cho, C. Park, and Y. Kim, "Flight Experiment on Separation and Reconstruction of Circular Formation by Decentralized System of Multiple Unmanned Aerial Vehicles," *Spring Conference of KSAS*, High One Resort, Gangwon-do, Korea, April 2015.

[18] C. Park, N. Cho, K. Lee, and Y. Kim, "Formation Flight of Multiple UAVs via Onboard Sensor Information Sharing," *Sensors*, Vol. 15, No. 7, 2015, pp. 17397-17419.

[19] C. Park, H. Kim, and Y. Kim, "Real-Time Leader-Follower UAV Formation Flight Based on Modified Nonlinear Guidance," *29th Congress of the International Council of the Aeronautical Sciences*, St. Petersburg, Russia, September 2014.

[20] G. Oh, C. Park, M. Kim, J. Park, and Y. Kim, "Small UAV System Identification in Time Domain," *Spring Conference of KSAS*, High One Resort, Gangwon-Do, Korea, April, 2012.

[21] H. Kim, M. Kim, H. Lim, C. Park, S. Yoon, D. Lee, H. Choi, G. Oh, J. Park, and Y. Kim, "Fully Autonomous Vision-Based Net-Recovery Landing System for a Fixed-Wing UAV," *IEEE/ASME Trans. Mechatronics*, Vol. 18, No. 4, 2013, pp. 1320–1332.

[22] S. Park, J. Deyst, and J. How, "Performance and Lyapunov Stability of a Nonlinear Path-Following Guidance Method," *Journal of Guidance, Control, and Dynamics*, Vol. 30, No. 6, 2007, pp. 1718–1728.

[23] D. Kim, S. Park, S. Nam, and J. Suk, "A Modified Nonlinear Guidance Logic for a Leader-Follower Formation Flight of Two UAVs," *International Conference on Control, Automation and Systems*, Fukuoka, Japan, August 2009.

[24] D. Lee, J. Lee, S. Kim, and J. Suk, "Design of a Track Guidance Algorithm for Formation Flight of UAVs," *Journal of Institute of Control, Robotics and Systems*, Vol. 20, No. 12, 2014, pp. 1217–1224.

[25] R. D. Williams, G. L. Feitshans, and A. J. Rowe, "A Prototype UAV Control Station Interface forAutomated Aerial Refueling," *AIAA Modeling and Simulation Technologies Conference*, San Francisco, CA, August 2005.

[26] B. Tucker and C. A. Ronald, "Behavior-based Formation Control for Multi-robot Teams," *IEEE Transeactions on Robotics and Automation*, Vol. 14, No. 6, 1998, pp. 926 - 939.

[27] L. Di, H. Chao, J. Han, and Y. Q. Chen, "Cognitive Multi-UAV Formation Flight: Principle, Low-Cost UAV Testbed, Controller Turning and Experiments," *ASME 2011 International Design Engineering Technical Conferences & Computers and Information in Engineering Conference*, Washington DC, August 2011.

[28] L. Schmitt and W. Fichter, "Collision-Avoidance Framework for Small Fixed-Wing Unmanned Aerial Vehicles," *Journal of Guidance, Control, and Dynamics*, Vol. 37, No. 4, 2014, pp. 1323-1328.

[29] F. Borrelli, T. Keviczky, and G. J. Balas, "Collision-free UAV Formation Flight Using Decentralized Optimization and Invariant Sets," *43rd IEEE Conference on Decision and Control*, Atlantis, Paradise Island, Bahamas, December 2004.

[30] V. Yadav and S. N. Balakrishnan, "Communication Control in Multiple UAV applications," *AIAA Guidance, Navigation, and Control Conference and Exhibit*, Keystone, Colorado, August 2006.

[31] J. Seo, C. Ahn, and Y. Kim, "Controller Design for UAV Formation Flight Using Consensus based Decentralized Approach," *AIAA Infotech@Aerospace Conference*, Seattle, Washington, April 2009.

[32] X. Wang, V. Yadav, and S. N. Balakrishnan, "Cooperative UAV Formation Flying With Obstacle/Collision Avoidance," *IEEE*

Transactions on Control Systems Technology, Vol. 15, No. 4, 2007, pp. 672-679.

[33] S. N. Singh and R. Zhang, "Decentralized Adaptive Close Formation Control of UAV's," *39th AIAA Aerospace Sciences Meeting*, Reno, Nevada, January, 2001.

[34] W. B. Randal, W. M. Timothy, and B. N. Derek, "Decentralized Cooperative Aerial Surveillance Using Fixed-Wing Miniature UAVs," *Proceedings of the IEEE,* Vol. 94, No. 7, 2006, pp. 1309-1324.

[35] R. Wei and W. B. Randal, "Virtual Structure based Spacecraft Formation Control with Formation Feedback," *AIAA Guidance, Navigation, and Control Conference and Exhibit*, Monterey, California, August 2002.

[36] P. Meir, J. D. John, and W. P. Andrew, "Tight Formation Flight Control," *Journal of Guidance, Control, and Dynamics,* Vol. 24, No. 2, 2001, pp. 246-254.

[37] H. V. Parunak, A. B. Sven, and J. O. James, "Swarming Coordination of Multiple UAV's for Collaborative Sensing," *2nd AIAA "Unmanned Unlimited" Systems, Technologies, and Operations*, San Diego, CA, September 2003.

[38] B. C. Henrik, J. P. Wayne, A. K. Adrian, K. K. Suresh, and N. J. Eric, "Small Adaptive Flight Control Systems for UAVs using FPGA/DSP Technology," *AIAA 3rd "Unmanned Unlimited" Technical Conference, Workshop and Exhibit*, Chicago, Illinois, USA, September 2004.

[39] N. H. M. Li and H. Liu, "Formation UAV Flight Control using Virtual Structure and Motion Synchronization," *IEEE American Control Conference*, Westin Seattle Hotel, Seattle, Washington, June 2008.

[40] A. C. Dixit, J. Falusi, S. Kim, G. Savit, and R. F. Stengel, "Integration of UAV in Flight and Ground Operations," *Guidance, Navigation, and Control and Co-located Conferences*, Boston, MA, August 2013.

[41] W. Ren and R. W. Beard, "Decentralized Scheme for Spacecraft Formation Flying via the Virtual Structure Approach," *Jounal of Guidance, Control, and Dynamics,* Vol. 24, No. 1, 2004, pp. 73-82.

[42] A. W. Lesley and E. H. John, "Decentralized Cooperative-Control Design for Multivehicle Formations," *Journal of Guidance, Control, and Dyanmicx,* Vol. 31, No. 4, 2008, pp. 970-979.

[43] G. Yu, M. R. Napolitano, and G. Campa, "3-Aircraft Formation Flight Experiment," *14th Mediterranean Conference on Control and Automation,* Ancona, Italy, June 2006.

[44] N. H. M. Li and H. H. T. Liu, "Multiple UAVs Formation Flight Experiments using Virtual Structure and Motion Synchronization," *AIAA Guidance, Navigation, and Control Conference,* Chicago, IL, August 2009.

국문초록

다수의 무인항공기를 이용하여 넓은 지역을 관찰하거나 여러 목표물을 동시에 감시하기 위해서는 복수 무인기의 편대 유도기법이 필요하다. 최근 복수 무인기 편대 유도기법에 관해 많은 연구들이 수행되어 왔으나, 대부분의 연구들이 다수 무인기의 통신에 적합하지 않은 중앙 집중형 통신기법을 기반으로 하였다. 또한, 알고리듬 검증을 위해 수치 시뮬레이션이나 무인기의 동특성을 반영할 수 없는 지상 로봇을 주로 사용하였다. 본 논문에서는 복수 무인기의 분산형 통신을 고려하였으며, 편대비행 유도 알고리듬의 성능을 수치 시뮬레이션뿐 아니라 비행실험을 통해 검증하였다.

본 논문에서는 복수 무인기의 자동 편대비행을 수행하기 위해 복수 무인기 시스템을 개발하고 편대 유도 알고리듬을 제안하였다. 기체 및 항공전자 시스템은 복수 무인기의 운용을 고려하여 적절하게 개발되었으며, 분산형 통신을 제안하여 무인기간 정보 공유 기법을 구현하고 성능을 검증하였다. 또한, 고정익 무인기의 동특성을 고려한 원형 편대비행과 근접 편대비행 알고리듬을 비선형 경로추종 유도기법 기반으로 제안하였다. 제안된 행동양식 기반 편대비행 기법과 선도-추종기 기반의 편대비행 기법은 수치 시뮬레이션을 통해 각 기법의 특성과 성능을 비교하였다.

제안된 알고리듬은 수치 시뮬레이션을 통하여 성능을 검증하였으며, 시뮬레이션 결과를 기반으로 복수의 무인기가 다양한 편대비행 임무를 수행할 수 있는 시나리오로 구성된 통합 편대 비행시험 계획을 수립하였다. 최종적으로 구축된 분산형 통신을 기반으로 한 복수 무인기 시스템과 편대비행 알고리듬은 통합비행시험을 통해 성능을 검증하였다.

주요어: 복수 무인기, 편대 비행, 분산형 통신기법, 근접 편대비행, 삼각 편대비행.

학번: 2009-20683